Executioner caspase is proximal to Fasciclin 3 which facilitates non-lethal activation in *Drosophila* olfactory receptor neurons

Authors

Masaya Muramoto[a,1], Nozomi Hanawa[a,1], Misako Okumura[b,c], Takahiro Chihara[b,c], Masayuki Miura[a,2], and Natsuki Shinoda[a,2]

Affiliations & Footnotes

[a] Department of Genetics, Graduate School of Pharmaceutical Sciences, University of Tokyo, 7-3-1 Hongo, Bunkyo-ku, Tokyo 113-0033, Japan

[b] Program of Biomedical Science, Graduate School of Integrated Sciences for Life, Hiroshima University, Higashi-Hiroshima, Hiroshima 739-8526, Japan

[c] Program of Basic Biology, Graduate School of Integrated Sciences for Life, Hiroshima University, Higashi-Hiroshima, Hiroshima 739-8526, Japan

[1] Equal contributions

[2] Corresponding authors

Corresponding Authors

Masayuki Miura: Department of Genetics, Graduate School of Pharmaceutical Sciences, University of Tokyo, 7-3-1 Hongo, Bunkyo-ku, Tokyo 113-0033, Japan. Telephone: +81-3-5841-4860. E-mail: miura@mol.f.u-tokyo.ac.jp

Natsuki Shinoda: Department of Genetics, Graduate School of Pharmaceutical Sciences, University of Tokyo 7-3-1 Hongo, Bunkyo-ku, Tokyo 113-0033, Japan. Telephone: +81-3-5841-4867. E-mail: f-shinoda.natsuki@g.ecc.u-tokyo.ac.jp

Abstract

The nervous system undergoes functional modification independent on cell turn over. Caspase participates in reversible neuronal modulation via non-lethal activation. However, the mechanism that enables non-lethal activation remains unclear. Here, we analyzed proximal proteins of *Drosophila* executioner caspase in the adult brain using TurboID. We discovered that executioner caspase Drice is, as an inactive proform, proximal to cell membrane proteins, including a specific splicing isoform of cell adhesion molecule Fasciclin 3 (Fas3), Fas3G. To investigate whether sequestration of executioner caspase to plasma membrane of axons is the mechanism for non-lethal activation, we developed a Gal4-Manipulated Area-Specific CaspaseTracker/CasExpress system for sensitive monitoring of caspase activity near plasma membrane. We demonstrated that *Fas3G*-overexpression promotes caspase activation in olfactory receptor neurons without killing them, by inducing expression of initiator caspase Dronc, which also comes close to Fas3G. Physiologically, *Fas3G* overexpression-facilitated non-lethal caspase activation suppresses innate olfactory attraction behavior. Our findings suggest that subcellularly-restricted caspase activation, defined by caspase proximal proteins, is the mechanism for non-lethal activation, opening the methodological development of reversible modification of neuronal function via regulating caspase proximal proteins.

Introduction

During and even after development, the nervous system undergoes functional modification usually not depending on cell turn over. Caspase, best known as a cysteine aspartic acid protease involved in cell death, participates neuronal functional modulation through non-lethal activation (Mukherjee and Williams, 2017). In zebrafish embryo, non-lethal caspase activity promotes axon arbor dynamics in retinal ganglion cells (Campbell and Okamoto, 2013). In *Drosophila*, caspase activation promotes engulfment of pruned dendrites during metamorphosis (Williams et al., 2006). Furthermore, non-lethal caspase activity promotes the maturation of olfactory sensory neurons during development in mice (Ohsawa et al., 2010). In the mature nervous system, non-lethal caspase activity induces long-term depression by AKT cleavage in mice (Li et al., 2010). These processes are termed caspase-dependent non-lethal cellular processes (CDPs)(Aram et al., 2017). While a growing number of CDPs have been identified (Nakajima and Kuranaga, 2017; Shinoda and Miura, 2024), relatively less is known about its regulatory mechanisms that enable specific non-lethal functions without causing cell death especially in nervous systems (Mukherjee and Williams, 2017). One potential mechanism is the restriction of the extent and spread of activated caspases (Mukherjee and Williams, 2017), yet experimental evidence is limited.

Proteins that interact with initiator caspases are among the key regulators of CDPs. Tango7, the *Drosophila* translation initiation factor eIF3 subunit m, acts as an adapter and regulates the localization of the initiator caspase Dronc. During sperm individualization, Tango7 directs Dronc to the individualization complex (D'Brot et al., 2013). In salivary glands, Tango7 directs Dronc to the plasma membrane (Kang et al., 2017). In both cases, caspase activity promotes cellular remodeling without inducing cell death (D'Brot et al., 2013; Kang et al., 2017). CRINKLED, a *Drosophila* unconventional myosin, functions as an adaptor of Dronc and facilitates the cleavage of Shaggy46 (Orme et al., 2016). Shaggy46, activated by caspase-

69 mediated cleavage, suppresses the emergence of ectopic sensory organ precursors (Kanuka et
70 al., 2005). During apoptosis-induced proliferation (AiP), Myo1D, another *Drosophila*
71 unconventional myosin, facilitates Dronc translocation to the basal side of the plasma
72 membrane of imaginal discs to promote AiP (Amcheslavsky et al., 2018). Thus, initiator
73 caspase-interacting proteins regulate caspase activity in CDPs. However, given the importance
74 of executioner caspases, which are activated by the initiator caspase to cleave a broad range of
75 substrates and are essential for apoptosis (Julien and Wells, 2017; Kumar, 2007), little is known
76 about the subcellular compartmentalization and interacting proteins of those involved in CDPs.
77 This lack of understanding is partly due to the absence of protein-protein interaction domains
78 (e.g., DED and CARD) in the N-terminus of executioner caspases (Kumar et al., 2022).

79 To understand the molecular mechanism regulating caspase activity involved in CDPs,
80 we focused on the proximal proteins of executioner caspases using TurboID, a proximity
81 labeling technique that analyzes protein proximity *in vivo* (Branon et al., 2018; Qin et al., 2021).
82 We have previously established C-terminal TurboID knocked-in caspase fly lines for Dronc
83 (initiator), Drice (executioner), and Dcp-1 (executioner) (Shinoda et al., 2019). Importantly, we
84 have demonstrated that one of the preferred substrates of Drice, BubR1, is proximal to Drice *in*
85 *vivo* (Shinoda et al., 2023), suggesting that substrate preference is exploited by protein
86 proximity. Therefore, the proximity of executioner caspases to proteins is emerging as a means
87 of regulating specific non-lethal functions.

88 To investigate the regulatory mechanisms of non-lethal function of caspase in the
89 nervous system, we conducted comprehensive analysis of proximal proteins of executioner
90 caspase Drice. We discovered that Drice is, as an inactive proform, primarily proximal to cell
91 membrane proteins, including cell adhesion molecule Fasciclin 3 (Fas3). Notably, Drice is
92 proximal to the specific alternative splicing isoforms of Fas3, Fas3G. To ascertain whether
93 Fas3G modulates caspase activity, we developed a Gal4-Manipulated Area Specific

94 CaspaseTracker/CasExpress (MASCaT) system, which permits the monitoring of caspase
95 activity near plasma membrane with high sensitivity and simultaneous genetic manipulation in
96 the cells of interest. Using MASCaT, we demonstrated that *Fas3G* overexpression enhances
97 caspase activation without killing olfactory receptor neurons through the induction of the
98 expression of initiator caspase Dronc, which also comes proximal to Fas3G. Subsequently, we
99 showed that *Fas3G* overexpression-facilitated non-lethal caspase activation in olfactory
100 receptor neurons suppresses innate olfactory attraction behavior. Collectively, our findings
101 suggest that caspase activation is subcellularly restricted, the platform of which is defined by
102 caspase proximal proteins, for non-lethal functions. In contrast to lethal activation, suppressing
103 neuronal activity with non-lethal caspase activation is reversible. By regulating caspase
104 proximal proteins, reversible modification of neuronal functional by non-lethal caspase
105 activation will be achieved.
106

107 **Results**

108 ***Drice is the major executioner caspase expressed in the adult brains***

109 Apoptotic stimuli activate initiator caspases that trigger a proteolytic cascade, leading to the
110 activation of executioner caspases and culminating in apoptosis (Green, 2019). In *Drosophila*,
111 the caspase-mediated apoptotic signaling pathway is highly conserved (Figure 1A) (Nakajima
112 and Kuranaga, 2017). The activity of executioner caspases, specifically Drice and Dcp-1, is
113 regulated by apoptotic signaling pathways, including the initiator caspase Dronc (Figure 1A).
114 To investigate the expression patterns of *Drosophila* caspases, we employed
115 *Caspase::V5::TurboID* knocked-in fly lines (Shinoda et al., 2019). We found low levels of
116 expression of the initiator caspase Dronc in adult heads (Figure 1B). Conversely, we observed
117 high expression of the executioner caspase Drice, whereas Dcp-1 was expressed at lower levels
118 in adult heads (Figure 1B). The proximal proteins of each caspase were labeled with TurboID
119 in adult heads by administration of 100 μM biotin (Figure 1B). Furthermore, we investigated
120 the expression patterns of caspases using histochemical analysis by examining streptavidin
121 (SA) signal. Consistent with the western blotting findings, Drice showed higher expression
122 levels than Dronc and Dcp-1, which were expressed at lower levels (Figure 1C). We found that
123 Drice was expressed in distinct regions, including the mushroom bodies (MBs), suboesophageal
124 ganglions (SOGs), optic lobes (OLs), and antennal lobes (ALs), which showed the highest
125 levels of expression (Figure 1C). The *Drosophila* ALs comprise synaptic contacts between the
126 axons of olfactory receptor neurons (ORNs), the dendrites of projection neurons (PNs), and
127 local interneuron (LNs) processes. Neuron-type-specific Gal4s were used to knockdown *Drice*
128 and the expression patterns were subsequently examined. We found that Drice was expressed
129 predominantly in ORNs in the AL (Figure 1D). These results show that Drice is highly
130 expressed in a specific subset of neurons in the adult brains. Comparisons of the expression
131 patterns of Drice were consistent across both males and females (Figure 1–figure supplement

132 1A, B), indicating an absence of sex-based differences, which justifies the use of males for
133 functional simplicity in this study.
134
135 ***Drice is proximal to cell membrane proteins rather than cytosolic proteins in the adult brains***
136 To comprehensively identify proximal proteins of Drice, we employed a proximity labeling
137 approach. Specifically, we used *Drice::V5::TurboID* knocked-in flies fed 100 μM biotin. We
138 confirmed biotinylation of Drice proximal proteins in the adult brains (Figure 1E). After
139 purifying the biotinylated proteins using NeutrAvidin magnetic beads, we performed LC-
140 MS/MS analysis of the samples (Figure 1F). We identified 643 proteins (Figure 1G, Table S1),
141 of which 158 were highly specific to *Drice::V5::TurboID* flies compared to wild-type flies
142 (*Drice::V5::TurboID*/w^{1118} > 10; Figure 1G, Table S1). Gene ontology analysis revealed that
143 Drice proximal proteins were enriched in the plasma membrane, synaptic vesicles, postsynaptic
144 membranes, and adherens junctions (Figure 1H, Table S2). This finding suggests that Drice is
145 localized primarily in cell membrane compartments rather than in the cytoplasm of the adult
146 brain. Additionally, because the SA signal of *Drice::V5::TurboID* is mainly observed in the
147 AL where the axons of ORNs project (Figure 1C), the enrichment of cell membrane proteins in
148 the proximal proteins of Drice is reasonable.
149
150 ***A specific splicing isoform of Fasciclin 3 is in proximity to Drice***
151 During our analysis of proteins proximal to Drice, we discovered that the expression patterns
152 of Fasciclin 3 (Fas3) in the adult brain closely resembled those of Drice, especially within the
153 OLs, SOGs, and ALs (Figure 2A, B). Thus, we focused on Fas3 (Chiba et al., 1995), a
154 transmembrane protein containing immunoglobulin-like domains that regulates synaptic target
155 recognition and axon fasciculation (Kose et al., 1997). *Fas3* is encoded by seven splicing
156 isoforms, resulting in the production of five protein isoforms that share extracellular domains

157 but differ in intracellular domains with low-complexity sequences (Figure 2C, D). Only one
158 specific protein isoform, Fas3 isoform G (Fas3G), was identified in the LC-MS/MS analysis as
159 a Drice-proximal protein in the adult brain (Figure 1G, Table S1). Using AlphaFold2-Multimer
160 (Evans et al., 2021; Mirdita et al., 2022), Drice was predicted to interact with Fas3A (ipTM =
161 0.456) and Fas3G (ipTM = 0.372) rather than Fas3C (ipTM = 0.298), Fas3D/E (ipTM = 0.220)
162 and Fas3B/F (ipTM = 0.207). Among Fas3 isoforms, only Fas3G is predicted to interact with
163 Drice with 2 intracellular regions (Figure 2–figure supplement 1A). To validate this result, we
164 generated an antibody specific to Fas3G (Figure 2C, E). We confirmed that only the Fas3G was
165 labeled with Drice::V5::TurboID and purified using NeutrAvidin magnetic beads as detected
166 using western blotting (Figure 2F). To further confirm the isoform specificity to Drice
167 proximity, we overexpressed 3xFLAG-tagged *Fas3 isoforms A*, *B/F*, *C*, *D/E*, and *G* in olfactory
168 receptor neurons using *Pebbled-Gal4* in a *Drice::V5::TurboID* knocked-in background. After
169 proximity labeling with TurboID, followed by NeutrAvidin purification, we found that the
170 Fas3G was highly enriched compared to the other isoforms (Figure 2G). These findings
171 suggested that Drice is proximal to a specific isoform of Fas3 in olfactory receptor neurons,
172 regardless of its protein expression level. We also investigated whether Drice and Fas3G
173 statically interact by co-immunoprecipitation. Although Fas3G was labelled by
174 Drice::V5::TurboID, indicating its proximity to Drice within the ORNs of adult brains, Drice
175 did not co-immunoprecipitate with Fas3G (Figure 2–figure supplement 2A). This result
176 suggests that while Drice and Fas3G are proximate, their interaction is not static, highlighting
177 the utility of proximity labeling as a superior technique to conventional co-immunoprecipitation
178 for identifying proteins that are spatially close.
179
180 ***Fasciclin 3s are not substrates of caspase***

181 It is often observed that proteins in close proximity to caspases are their preferred substrates
182 (Shinoda et al., 2023). To investigate this, we examined whether any of the Fas3 isoforms are
183 substrates for caspase by expressing all isoforms in *Drosophila* S2 cells. However, we found
184 that none of the Fas3 isoforms were cleaved by caspase following the induction of apoptosis
185 (Figure 2–figure supplement 2B). Therefore, Fas3s are not substrates of caspase.
186
187 ***MASCaT: a cell type-specific highly sensitive caspase activity reporter***
188 We investigated whether Fas3G regulates caspase activity in lethal or non-lethal processes.
189 CaspaseTracker/CasExpress is a highly sensitive reporter of caspase activity that uses caspase-
190 activatable Gal4 tethered to the membrane by mCD8 (Ding et al., 2016; Tang et al., 2015).
191 However, reliance on Gal4 to report their activity presents a challenge in reconciling
192 Gal4/UAS-dependent gene manipulations. To overcome this limitation, we created a new
193 reporter to capture caspase activation independent of caspase-activatable Gal4. We replaced the
194 caspase-activatable Gal4 with the caspase-activatable QF2 (*mCD8::DQVD::QF2*), where
195 DQVD is a caspase cleavage sequence, and first expressed directly downstream of *UAS*
196 sequence (Figure 3–figure supplement 1A). However, the caspase-activatable QF2 induced
197 mNeonGreen expression under *QUAS* sequence even either with a pan-caspase inhibitor,
198 zVAD-fmk, or an uncleavable DQVA mutant probe (*mCD8::DQVA::QF2*, insensitive to
199 caspase-mediated cleavage which serves as a negative control) (Figure 3–figure supplement
200 1B), potentially because the Gal4/UAS binary system expressed excessive
201 mCD8::DQVD/A::QF2 probes that results in caspase activation-independent induction of
202 QF2/QUAS system. Thus, to reduce the amount of probes expression, we generated *Ubi-FRT-*
203 *STOP-FRT-mCD8::DQVD::QF2*, simultaneously expressing *Flippase* (*FLP*) under *UAS* to
204 restrict reporter expression to the cells of interest (Figure 3A). *Drosophila* S2 cells undergo
205 weak caspase activation only by transfection (Shinoda et al., 2023). Taking advantage of that,

206 this system reports caspase activity through the caspase-activatable QF2/QUAS system,
207 expressing mNeonGreen, which is not detected by caspase-non-activatable QF2 (Figure 3B).
208 We named this novel reporter a Gal4-Manipulated Area Specific CaspaseTracker/CasExpress
209 (MASCaT; Figure 3A). Using MASCaT, we detected caspase activity, specifically in the
210 neurons of adult brains, using *ELAV-Gal4* (Figure 3C). Caspase activity was prominent in OLs
211 (Figure 3C), which is consistent with the previously reported activation pattern of caspase
212 detected by CaspaseTracker/CasExpress (Ding et al., 2016; Tang et al., 2015). Previously, we
213 reported that a specific subset of ORNs, including Or42b neurons, undergoes age-associated
214 caspase activation (Chihara et al., 2014). Consistent with this finding, we detected age-
215 dependent caspase activation in the AL (Figure 3C). We further confirmed the age-dependent
216 caspase activation in Or42b neurons (Figure 3D). Therefore, our newly established reporter,
217 MASCaT, enables the highly sensitive detection of caspase activity near the plasma membrane
218 in cells of interest reconciling with Gal4/UAS-dependent gene manipulations.
219
220 ***Fas3G overexpression activates caspase in a non-lethal manner***
221 To investigate the regulatory role of Fas3 in caspase activity *in vivo*, we used Or42b neurons as
222 a model, which have previously been shown to undergo age-dependent caspase activation
223 (Chihara et al., 2014). Initially, we evaluated the effects of *Dronc* overexpression on apoptosis
224 by quantifying cell body numbers in the antenna in young flies. Dronc induced cell loss while
225 catalytically inactive Dronc ($Dronc^{CG}$) did not, suggesting that Dronc induce apoptosis in a
226 catalytic-dependent manner (Figure 4A, B). We then evaluated the effects of the overexpression
227 of the executioner caspases *Dcp-1* and *Drice*. Interestingly, although Dcp-1 induced complete
228 cell loss, Drice did not (Figure 4A, B), suggesting that Drice requires an initiator caspase for
229 activation, whereas Dcp-1 does not. These results indicate that Or42b neurons are competent in
230 caspase-mediated cell loss and thus serve as a model for evaluating apoptosis. However, the

231 expression of *Fas3G*, even in combination with *Drice*, did not reduce the number of cells,
232 implying that *Fas3G* overexpression did not induce apoptosis (Figure 4C, D).

233 Subsequently, we assessed the regulation of non-lethal caspase activity by Fas3G *in*
234 *vivo*. We first confirmed that MASCaT probes were distributed in the axons of ORNs (Figure
235 4E). Using MASCaT, we observed weak caspase activation even in the control group at a young
236 age (Figure 4F, G). The expression of *Fas3G* significantly promoted caspase activation (Figure
237 4F, G), indicating that Fas3G regulates non-lethal caspase activation. Moreover, the
238 simultaneous expression of *Drice* and *Fas3G* significantly enhanced caspase activation (Figure
239 4F, G), signifying the promoting effect of their proximity. Moreover, the concurrent expression
240 of Diap-1, an E3 ligase known to inhibit caspase activation (Ditzel et al., 2008; Hay et al., 1995;
241 Lee et al., 2011), mitigated the caspase activation induced by *Fas3G* overexpression (Figure
242 4H, I). This indicates that *Fas3G* overexpression-facilitated non-lethal caspase activation is
243 dependent on the core apoptotic machinery. To test whether endogenous Fas3G regulates
244 caspase activation, we generated *Fas3G*-specific *shRNA* expressing strain (Figure 4–figure
245 supplement 1A, B). Knockdown of *Fas3* or *Fas3G* in Or42b neurons didn't suppress the
246 inherent, weak caspase activation (Figure 4–figure supplement 1C, D). In agreement with this,
247 Drice's presence in the axon of ORNs with Fas3G was observed, yet its presence was not strictly
248 contingent on Fas3 or Fas3G (Figure 4–figure supplement 1E). Given the numerous other
249 membrane proteins in proximity to Drice (Figure 1G, H and Table S1), it is probable that
250 additional proteins may be responsible for recruiting Drice to the axon. These findings
251 collectively imply that while Fas3G is not essential for mild endogenous caspase activation,
252 overexpression of *Fas3G* does enhance non-lethal caspase activation in ORNs, thus providing
253 a valuable model for exploring the molecular processes that facilitate caspase activation without
254 leading to cell death.
255

256 ***Fas3G is proximal to Dronc which is required for non-lethal caspase activation***

257 Next, we investigated the underlying mechanism that enhances non-lethal activation facilitated
258 by *Fas3G* overexpression. Executioner caspases, Drice and Dcp-1, are activated by initiator
259 caspases, Dronc (Figure 1A). We precisely analyzed expression pattern of Dronc in adult brains
260 and found that while its expression was low in control, overexpression of *Fas3G* in ORNs
261 markedly increased Dronc levels in those neurons (Figure 5A). Moreover, akin to Drice, Dronc
262 was also found in close proximity to the overexpressed Fas3G, but not to the overexpressed
263 Fas3C in ORNs (Figure 5B). Consequently, we examined whether Dronc is required for the
264 non-lethal caspase activation enhanced by *Fas3G* overexpression. Employing MASCaT, we
265 discovered that both knockdown of *Dronc* and the expression of the *dominant-negative form of*
266 *Dronc* (*Dronc*^{DN}) hindered the non-lethal caspase activation facilitated by *Fas3G*
267 overexpression (Figure 5C, D), indicating a dependence on initiator caspase activity.
268 Importantly, the genetic suppression of Dronc activity did not alter the proximity between Drice
269 and Fas3G (Figure 5E), suggesting that the inactive Drice proform is primarily proximal to
270 Fas3G. Solo overexpression of *Dronc* led to cell death in Or42b neurons (Figure 4A, B),
271 whereas *Fas3G* overexpression elevated Dronc expression without causing cell death (Figure
272 4C, D, Figure 5A). Collectively, these findings imply that the non-lethal caspase activation
273 driven by *Fas3G* overexpression is orchestrated by an increase in Dronc induced by Fas3G,
274 bringing Dronc in close vicinity to Fas3G and thus enabling caspase activation near the plasma
275 membrane (Figure 5F).

276

277 ***Non-lethal caspase activation regulates innate attraction behavior***

278 Finally, we examined the function of *Fas3G* overexpression-facilitated non-lethal caspase
279 activation. Apple cider vinegar (ACV) excites six glomeruli in the AL, including DM1, which
280 is innervated by the axons of Or42b neurons (Semmelhack and Wang, 2009). We have

281 previously reported that Or42b neurons undergo aging-dependent caspase activation and partial
282 cell death, which reduces neuronal activity and attraction behavior in response to ACV (Chihara
283 et al., 2014). Inhibition of caspase activity in aged flies restores attraction behavior but does not
284 affect that of young flies (Chihara et al., 2014). Using a two-choice preference assay with ACV
285 (Figure 6A), we found that 16 hours of starvation combined with 25% ACV in the trap elicited
286 a robust attraction behavior to the vinegar (Figure 6B). In contrast, 4 hours of starvation with
287 1% ACV in the trap resulted in milder attraction behavior, with the preference index value being
288 close to 0 but still showing a positive trend (Figure 6B). Under the milder experimental
289 condition, we first confirmed that inhibition of caspase activity through expressing *Dronc*^{DN}
290 didn't affect attraction behavior in young adult (Figure 6C), consistent with a previous report
291 (Chihara et al., 2014).We then observed that the overexpression of *Fas3G*, which activates
292 caspases, did not impair attraction behavior. Instead, it rather appeared to enhance the tendency
293 for attraction behavior (Figure 6C), suggesting that Fas3G promotes attraction behavior. Finally,
294 we found that inhibiting *Fas3G* overexpression-facilitated non-lethal caspase activation by
295 expressing *Dronc*^{DN} strongly promoted attraction to ACV (Figure 6C). Overall, these results
296 suggest that *Fas3G* overexpression has a dual function: it enhances attraction behavior while also
297 triggering non-lethal caspase activation, which counteracts the behavioral response, functioning
298 as a regulatory brake without causing cell death.
299

300 **Discussion**

301 ***Proximal proteins of executioner caspases regulate non-lethal caspase activity***

302 It is important to identify the proximal proteins of executioner caspases, which cleave a wide
303 range of substrates and are essential for apoptosis (Julien and Wells, 2017; Kumar, 2007), as
304 proximity often dictates substrate specificity (Shinoda et al., 2023). In humans, caspase-3 and
305 caspase-7 have been shown to share but also have discrete substrate preferences (Walsh et al.,
306 2008). Caspase-7 leverages an exosite to facilitate interaction with RNA and enhance the
307 proteolysis of RNA-binding proteins (Boucher et al., 2012; Desroches and Denault, 2019). Thus,
308 protein proximity can be used to precisely regulate specific cellular functions by selectively
309 cleaving a limited pool of substrates in non-lethal scenarios compared with lethal cleavages
310 where all the substrates are potentially cleaved during apoptosis. We showed that executioner
311 caspases, before activation as proforms, are exclusively sequestered in specific subcellular
312 domains, including the plasma membrane of axons. We found that *Fas3G* overexpression
313 facilitates non-lethal activation, underscoring the importance of protein proximity not only in
314 substrate cleavage, but also in localizing non-lethal activation to the vicinity of plasma
315 membrane of axons (Figure 5F). Our results suggest that subcellularly restricted caspase
316 activation mediated by caspase proximal proteins is one of the potential mechanisms regulating
317 caspase activation without inducing cell death.

318

319 ***MASCaT as a highly sensitive reporter for identifying non-lethal caspase regulators***

320 Various caspase activity reporters have been developed, including SCAT3, a FRET-based
321 reporter with superior temporal resolution (Takemoto et al., 2003), CaspaseTracker/CasExpress,
322 Caspase-activatable Gal4-based reporters with superior sensitivity (Ding et al., 2016; Tang et
323 al., 2015). However, to date, no reporter has been developed that is sensitive enough to identify
324 non-lethal regulators of caspases in cells of interest. In this study, we developed a novel caspase

325 reporter, MASCaT, that can detect caspase activation with high sensitivity in a cell type-specific
326 manner following gene manipulation. Using MASCaT, we identified previously overlooked
327 regulators of non-lethal activation of caspases in a cell type-specific manner. Proximal proteins
328 of executioner caspases are potential non-lethal regulators, and combining TurboID-mediated
329 identification of these proteins will pave the way for identifying non-lethal components and
330 broaden our understanding of the molecular mechanism of non-lethal caspase activation.
331
332 ***Non-lethal caspase activation regulates neuronal activity and behaviors***
333 We previously reported that age-dependent caspase activation reduces neuronal activity and
334 innate attraction behavior (Chihara et al., 2014). Here, we found that, while *Fas3G*
335 overexpression did not impair attraction behavior by itself, caspase activation upon *Fas3G*
336 overexpression suppressed attraction behavior toward ACV (Figure 6C). In mice, L1CAM, an
337 immunoglobulin-like cell adhesion molecule similar to Fas3, facilitates neuronal excitability
338 by regulating the voltage-gated Na+ channels (Valente et al., 2016). Thus, we hypothesize that
339 non-lethal caspase activation antagonizes the neuronal excitability promoted by Fas3G. In
340 neurons, caspases have diverse non-lethal functions, including axon degeneration and macro-
341 and micro-pruning, to regulate synaptic plasticity (Dehkordi et al., 2022; Mukherjee and
342 Williams, 2017). In presynaptic terminals, it has been recently reported that Caspase-3
343 modulates synaptic vesicle pools via autophagy (Gu et al., 2021). Thus, it is possible that non-
344 lethal activation regulates synaptic pools and neuronal activity in a reversible manner without
345 killing the cells. Analyzing the functions mediated by Drice and Fas3G proximity, including
346 the identification of specific substrates, will pave the way for identifying diverse CDPs and
347 understanding their molecular mechanisms.
348 While suppressing innate attraction behavior does not seem beneficial by itself, it
349 should be a great advantage in decision-making. To survive, flies must constantly make

350 appropriate behavioral decisions (e.g., feeding versus mating) depending on their physiological
351 conditions. In males, a subset of neurons regulated by tyramine controls feeding versus mating
352 behaviors (Cheriyamkunnel et al., 2021). In regard of that, it is important to adequately promote
353 or suppress neuronal activity, which controls behaviors of the organisms, by precisely
354 controlling caspase activation in a subcellularly restricted manner in neurons. Compared with
355 lethal activation which irreversibly removed the neurons of interest, suppressing neuronal
356 activity with non-lethal reversible caspase activation is beneficial for decision makings
357 depending on their varying physiological conditions. As regulating caspase proximal proteins
358 enables non-lethal activation which is not achieved by directly manipulating caspase expression,
359 our results open the possibility of the methodological development for reversible manipulation
360 of neuronal activity via non-lethal caspase activity.
361
362 ***Proximal proteins of executioner caspases define the site of caspase activation "hotspot"***
363 Although the core apoptotic machinery has been well characterized during the last 30 years
364 (Nakajima and Kuranaga, 2017; Shinoda and Miura, 2024), the precise regulation of CDPs,
365 remains incompletely elucidated. In this study, we identified *Fas3G* overexpression activates
366 Drice. Mechanistically, we found that *Fas3G* overexpression induced the expression of initiator
367 caspase Dronc, which also comes close to Fas3G, regulating non-lethal caspase activation.
368 Direct overexpression of Dronc alone results in cell death within olfactory receptor neurons
369 (Figure 4A, B). However, when Dronc expression is upregulated due to *Fas3G* overexpression,
370 it does not lead to cell death in ORNs (Figure 4C, D). The exact process by which Dronc
371 expression is increased in response to *Fas3G* overexpression remains to be elucidated. It is
372 known that Dronc can be upregulated via the ecdysone signaling pathway (Dorstyn et al., 1999)
373 and the Hippo signaling pathway (Verghese et al., 2012). Therefore, the overexpression of
374 *Fas3G* might potentially activate Dronc expression through one or both signaling pathways.

375 Fas3 is an immunoglobulin-like domain-containing transmembrane protein that regulates
376 axonal fasciculation and neuronal projections (Chiba et al., 1995). NCAM, a mammalian
377 homologue of Fascicilin 2, is an immunoglobulin-like domain-containing cell adhesion
378 molecule. NCAM can physically bind to caspase-8, and depending on NCAM clustering,
379 caspase-8 and -3 are activated and contribute to neurite outgrowth by cleaving its substrate
380 spectrin (Westphal et al., 2010). Thus, it seems likely that cell adhesion molecule-mediated
381 subcellularly restricted caspase activation is conserved among species. Indeed, caspase-9/Apaf-
382 1-dependent caspase-3 activation, without resulting in cell death, has also been observed in the
383 axon of olfactory sensory neurons during mouse development (Ohsawa et al., 2010).

384 While the restriction of the extent and spread of activated caspases is proposed as one
385 of the potential molecular mechanisms for non-lethal activation (Mukherjee and Williams,
386 2017), experimental evidences are limited. A critical insight from our research is that the
387 executioner caspase is pre-compartmentalized in proximity to a specific set of proteins prior to
388 activation, poised for the initiator caspase to approach. Consequently, the "hotspot" for non-
389 lethal caspase activity appears to be determined by these neighboring proteins of executioner
390 caspases. While the "hotspot" located in the axon of the ORN may exert an inhibitory effect on
391 neuronal activity, it could also play a role in avoiding cell death by localizing caspase activity,
392 especially during development.

393 Recently, a protein interactome analysis in humans showed that tissue-preferentially
394 expressed proteins that interact with known apoptosis regulators participate in apoptosis
395 sensitization (Luck et al., 2020). Given that CDPs are often cell-and tissue type-specific
396 processes, the identification of modulators of context-dependent apoptotic pathways will aid in
397 understanding the precise molecular regulation of CDPs. Importantly, alternative splicing can
398 diversify protein-protein interaction networks. A recent report showed that minor spliceosomes
399 regulate alternative splicing, including Fas3. A specific isoform of Fas3 has distinct functions

400 and cannot be substituted by other isoforms during neuronal development (Li et al., 2020). Our
401 results support the idea that alternative splicing may not only diversify the protein itself, but
402 also its interaction networks to regulate module-dependent activation. Further interactome
403 analysis using TurboID will reveal the regulatory mechanisms of the non-lethal activation of
404 caspases.
405

406 **Methods**

407 ***Fly strains and rearing conditions***

408 We raised the flies in standard *Drosophila* medium at 25°C. For in vivo biotin labeling
409 experiments, flies were raised in standard *Drosophila* medium supplemented with 100 μM (+)-
410 biotin (#132-02635, WAKO) for at least 5 days. The fly strains used in this study are listed in
411 Table S3. The detailed genotypes corresponding to each figure are provided in Table S4.

412

413 ***Protein preparation from Drosophila tissues***

414 Adult heads or brains of the given genotype were dissected in phosphate-buffered saline (PBS)
415 and lysed with RIPA buffer (50 mM Tris-HCl, pH 8.0, 150 mM Sodium Chloride, 0.5 w/v%
416 Sodium Deoxycholate, 0.1% w/v Sodium Dodecyl Sulfate, and 1.0% w/v NP-40) supplemented
417 with cOmplete ULTRA EDTA-free protease inhibitor cocktail (#05892953001, Roche).
418 Samples were homogenized and centrifuged at 20,000 ×g, 4°C for 10 min. The supernatants
419 were collected and snap-frozen in liquid nitrogen. Protein concentrations were determined
420 using the BCA assay (#297-73101, WAKO) following the manufacturer's protocol. The
421 samples were mixed with 6x Laemmli buffer, boiled at 95°C for 5 min, and then subjected to
422 purification of biotinylated proteins and western blot analysis.

423

424 ***Western blotting***

425 Each sample was separated using SDS-PAGE. The proteins were then transferred onto
426 Immobilon-P PVDF membranes (#IPVH00010; Millipore) for immunoblotting. Membranes
427 were blocked with 4% skim milk diluted in 1× TBST. Immunoblotting was performed using
428 the antibodies mentioned below diluted in 4% skim milk diluted in 1× TBST. Signals were
429 visualized using Immobilon Western Chemiluminescent HRP Substrate (#WBKLS0500;

430 Millipore) and FUSION SOLO. 7S. EDGE imaging station (Vilber-Lourmat). Contrast and
431 brightness adjustments were applied equally using Fiji (ImageJ) software (NIH Image).
432 The primary antibodies used included mouse anti-V5 monoclonal antibody (1:5,000,
433 #46-0705, Invitrogen), mouse anti-FLAG M2 monoclonal antibody (1:5,000, Sigma), mouse
434 anti-alpha tubulin (DM1A) monoclonal antibody (1:10,000, #T9026, Sigma), mouse anti-Actin
435 monoclonal antibody (1:5,000; #A4700, Sigma), mouse anti-Fasciclin 3 (7G10) antibody (1:50,
436 #AB_528238, DSHB), rabbit anti-Fasciclin3 isoform G antibody (1:50, this study), mouse anti-
437 Drosophila Lamin B monoclonal antibody (1:1000, #ADL67.10, DSHB). The secondary
438 antibodies used included goat anti-rabbit IgG HRP-conjugated antibody (1:5,000, #7074S,
439 CST) and goat/rabbit/donkey anti-mouse IgG HRP Conjugate (1:5,000, #W402B, Promega).
440 The membranes for streptavidin blotting were blocked with 3% BSA diluted in 1× TBST.
441 Streptavidin blotting was performed using streptavidin-horseradish peroxidase (1:10,000,
442 #SA10001; Invitrogen) diluted in 3% BSA diluted in 1× TBST.
443
444 ***Co-immunoprecipitation***
445 Adult heads were lysed on ice using DDM IP lysis buffer (50 mM Tris-HCl (pH 7.5), 150 mM
446 NaCl, 0.2% N-Dodecyl-β-D-maltoside (DDM) (#341-06161, WAKO)) containing cOmplete
447 ULTRA EDTA-free protease inhibitor cocktail. The samples were adjusted to 150 μg
448 protein/150 μL DDM IP lysis buffer. The samples were incubated overnight at 4 °C with 10
449 μL anti-FLAG M2 Magnetic Beads (#M8823-1ML, Millipore) equilibrated with the DDM IP
450 lysis buffer. The beads were washed three times in wash buffer (50 mM Tris-HCl (pH 7.5),
451 150 mM NaCl, 0.1% DDM) and boiled for 5 min at 95 °C with 50 μL 1× Laemmli buffer. The
452 samples were magnetically separated, and the supernatants were subjected to SDS-PAGE.
453
454 ***Immunohistochemistry***

455 Adult brains were dissected in PBS and fixed in 4% paraformaldehyde (PFA) at room
456 temperature for 30 min. Adult brains were washed three times with 0.3% PBST (Triton-X100)
457 for 10 min. After blocking with 5.0% normal donkey serum (#S30, Millipore)/PBST (PBSTn)
458 for 30 minutes at room temperature, tissues were incubated with primary antibody/PBSTn
459 overnight at 4°C. The samples were then washed with PBST three times for 10 min each and
460 incubated with secondary antibody/PBSTn for 2 h at room temperature. After incubation, the
461 tissues were washed with PBST three times for 10 min. Streptavidin and Hoechst 33342 were
462 added during secondary antibody incubation. The samples were mounted on glass slides with
463 SlowFade Gold antifade reagent (#S36939, Invitrogen). Images were captured using a Leica
464 TCS SP8 microscope (Leica Microsystems). Images were analyzed and edited using the Fiji
465 (ImageJ) software. For MASCaT analysis, newly eclosed adults were raised at 29°C for 1 week.
466 Classification of the MASCaT signal was performed by optically assessing the tdTomato
467 intensity. For cell number analysis, newly eclosed adults were raised at 29°C for 1 week. The
468 antennae were dissected as previously described (Karim et al., 2014), fixed with 4% PFA at
469 room temperature for 30 min, and washed with 0.4% PBST (Triton-X100) three times for 10
470 min. Quantification of cell numbers in antenna was performed using Fiji (ImageJ) software
471 using "3D object counter" for RedStinger positive cells.

472 The primary antibodies used were mouse anti-Fasciclin 3 (7G10) antibody (1:20,
473 #AB_528238, DSHB), rat anti-GFP (GF090R) monoclonal antibody (1:100, #04404-26,
474 nacalai Tesque), mouse anti-FLAG M2 monoclonal antibody (1:500, F1804, Sigma), and rat
475 anti-mCD8 monoclonal antibody (1:50, #MCD0800, Invitrogen). The secondary antibodies
476 used included Alexa Fluor 488-conjugated donkey anti-mouse IgG antibody (1:500, #A-21202,
477 ThermoFisher Scientific), Alexa Fluor 488-conjugated donkey anti-rat IgG antibody (1:500,
478 #A-21208, ThermoFisher Scientific), Alexa Fluor 647-conjugated donkey anti-mouse IgG
479 antibody (1:500, #A-31571, ThermoFisher Scientific), and Alexa Fluor 633-conjugated goat

480 anti-rat IgG antibody (1:500, #A-21094, ThermoFisher Scientific). The nuclei were stained
481 with Hoechst 33342 (8 μM, #H3570, Invitrogen). Streptavidin-Cy2 (1:500, #016-220-084,
482 Jackson ImmunoResearch) and Streptavidin-Cy5 (1:500, #016-170-084, Jackson
483 ImmunoResearch) were used to stain the biotinylated proteins.
484
485 ***Experimental design for liquid chromatography-tandem mass spectrometry (LC-MS/MS)***
486 ***analyses***
487 Two biological replicates were analyzed for each experimental condition to determine the
488 relative abundance of *Drice::V5::TurboID/w*^{1118}.
489
490 ***Purification of biotinylated proteins***
491 Samples were prepared as previously described (Shinoda et al., 2023). Briefly, 100 μg of
492 biotinylated protein-containing lysate (from 100 brains or 20 heads) was subjected to FG-
493 NeutrAvidin bead (#TAS8848 N1171, Tamagawa Seiki) purification. The FG-NeutrAvidin
494 beads (25 μL, approximately 500 μg) were washed three times with RIPA buffer. Benzonase-
495 treated biotinylated protein samples suspended in 1 mL RIPA buffer were incubated overnight
496 at 4°C. Conjugated beads were magnetically isolated and washed with 500 μL of an ice-cold
497 RIPA buffer solution, 1 M KCl solution, 0.1 M Na_2CO_3 solution and 4 M urea solution. For
498 western blot analyses, the purified samples were mixed with Laemmli buffer, boiled at 95°C
499 for 5 min, and then subjected to western blot analysis. For LC-MS/MS analysis, the purified
500 samples were washed with 500 μL ultrapure water (#214-01301, WAKO) and 500 μL of 50
501 mM ammonium bicarbonate (AMBC). The samples were then mixed with 50 μL of 0.1%
502 Rapigest diluted in 50 mM AMBC, and 5 μL of 50 mM TCEP was subsequently added.
503 Samples were incubated at 60°C for 5 min, and then 2.5 μL 200 mM MMTS was added. One
504 microgram sequence-grade modified trypsin (#V5111, Promega) was then added for on-bead

505 trypsin digestion at 37°C for 16 h. The beads were magnetically isolated and 60 µL of the
506 supernatant was collected. Then, 3 µL 10% TFA was added to the supernatants, and the samples
507 were incubated at 37°C for 60 min with gentle agitation. The samples were then centrifuged at
508 20,000 ×g, 4°C for 10 min. The peptides were desalinated and purified using a GL-tip SDB
509 (#7820-11200, GL Sciences) following the manufacturer's protocol. The samples were speed-
510 backed at 45°C for 30 min and dissolved in 25 µL of 0.1% formic acid. The samples were then
511 centrifuged at 20,000 ×g, 4°C for 10 min, and the supernatants were collected. The peptide
512 concentrations were determined using the BCA assay. Finally, 500 ng of the purified protein
513 was subjected to LC-MS/MS analysis.
514
515 ***LC-MS/MS analyses***
516 LC-MS/MS analyses were performed as previously described (Shinoda et al., 2023). Briefly,
517 samples were loaded onto Acclaim PepMap 100 C18 column (75 µm x 2 cm, 3 µm particle size
518 and 100 Å pore size; #164946, ThermoFisher Scientific) and separated on nano-capillary C18
519 column, (75 µm x 12.5 cm, 3 µm particle size, #NTCC-360/75-3-125, Nikkyo Technos) using
520 EASY-nLC 1200 system (ThermoFisher Scientific). The elution conditions are listed in Table
521 S5. The separated peptides were analyzed using QExactive (ThermoFisher Scientific) in data-
522 dependent MS/MS mode. The parameters for the MS/MS analysis are listed in Table S6. The
523 collected data were analyzed using Proteome Discoverer (PD) 2.2 software with the Sequest
524 HT search engine. The parameters for the PD 2.2 analysis are described in Table S7. Peptides
525 were filtered at a false discovery rate of 0.01 using the Percolator node. Label-free
526 quantification was performed based on the intensities of the precursor ions using a precursor-
527 ion quantifier node. Normalization was performed using the total amount of peptides in all
528 average scaling modes. Proteins with 10 folds or higher abundance relative to the control (w^{1118})
529 were considered for further analysis. MS proteomic data were deposited in the

530 ProteomeXchange Consortium via the jPOST partner repository with the dataset identifier
531 PXD042922 (Okuda et al., 2017).
532
533 ***Gene Ontology analysis***
534 Gene Ontology (GO) analysis of cellular components was performed using DAVID (Huang et
535 al., 2009).
536
537 ***Generation of rabbit polyclonal anti-Fasciclin 3 isoform G antibody***
538 The peptide corresponding to the 506–524 AA (N-LKPANEATPATTPAPTTAA-C) of Fas3G
539 was used by Eurofins Inc. to immunize rabbits to raise a polyclonal antibody. The antibody was
540 affinity purified using the same peptide provided by Eurofins, Inc.
541
542 ***IDR prediction***
543 Amino acid sequences were obtained from the FlyBase database [https://flybase.org/].
544 Disordered intracellular regions of Fas3 isoforms were predicted using the PSIPRED protein
545 sequence analysis workbench in DISOPRED3 [http://bioinf.cs.ucl.ac.uk/psipred/].
546
547 ***Protein complexes prediction with AlphaFold2-Multimer***
548 Amino acid sequences were obtained from the FlyBase database [https://flybase.org/]. Protein
549 complexes were predicted using ColabFold v1.5.5: AlphaFold2 using MMseqs2 (Mirdita et al.,
550 2022) with the following settings: template_mode:none, msa_mode: mmseqs2_uniref_env,
551 pair_mode: unpaired_paired, model_type: alphafold2_multimer_v3, num_recycles: 3. PAE
552 plots of the structural models ranked first among five models were selected as representatives.
553
554 ***Molecular cloning***

555 For all isoforms (A, B/F, C, D/E, G) of *pUASz-Fasciclin 3::3xFLAG*, the coding sequences of
556 Fasciclin 3s were PCR-amplified using 3xFLAG-tag harboring primers from *Drosophila* cDNA
557 and were ligated into the *Bam*HI/*Kpn*I-digested *pUASz1.0* vector (#1431, *Drosophila* Genomics
558 Resource Center (DGRC)) (DeLuca and Spradling, 2018) using In-Fusion (#Z9648N,
559 TaKaRa). For all isoforms of *pAc5-Fasciclin 3::3xFLAG*, the coding sequence of *Fasciclin*
560 *3s::3xFLAG* were PCR-amplified from corresponding *pUASz-Fasciclin 3::3xFLAG* vectors
561 and were ligated into the *Eco*RI/*Xho*I-digested *pAc5-STABLE2-neo* vector (#32426, Addgene)
562 (González et al., 2011) using NEBuilder HiFi DNA Assembly (#E2621L, NEB). For *pUASz-*
563 *3xFLAG::mNeonGreen*, the coding sequence of mNeonGreen was PCR-amplified using
564 3xFLAG-tag harboring primers from *pAc5-V5::mNeonGreen* (Shinoda et al., 2023) and ligated
565 into the *Xho*I-digested *pUASz1.0* vector using In-Fusion. For *pUASz-*
566 *Drice::myc::mNeonGreen*, the coding sequence of mNeonGreen was PCR-amplified from
567 *pAc5-V5::mNeonGreen* using myc-tag-harboring primers. The coding sequence of Drice was
568 PCR-amplified from *Drosophila* cDNA. The two fragments were then ligated into the *Xho*I-
569 digested *pUASz1.0* vector using In-Fusion. For *pUASz-V5::TurboID* and *pUASz-*
570 *Caspase::V5::TurboID*, the coding sequences of *Dcp-1*, *Drice* and *Dronc* were PCR amplified
571 from *Drosophila* cDNA. The coding sequence of V5::TurboID was PCR-amplified from *V5-*
572 *TurboID-NES_pcDNA3* (#107169; Addgene). The two fragments were then ligated into the
573 *Xho*I-digested *pUASz1.0* vector using In-Fusion. Catalytic dead mutations (Dcp-1: C196G
574 (TGC to GGC), Drice: C211G (TGC to GGC), and Dronc: C318G (TGC to GGC)) were
575 introduced by PCR-based site-directed mutagenesis, and the corresponding fragments were
576 ligated into the *Xho*I-digested *pUASz1.0* vector using In-Fusion. For *pJFRC-*
577 *mCD8::DQVD/A::QF2*, the coding sequence of *mCD8::DQVD/A* were PCR-amplified from
578 genomic DNA of *Caspase-Sensitive/Insensitive-Gal4* (Tang et al., 2015). The coding sequence
579 of *QF2* was PCR-amplified from *pBPQU* vector (Kashio et al., 2016). These fragments were

580 ligated into the *Xho*I/*Xba*I-digested *pJFRC-28K* vector (a gift from H. Kazama) using In-
581 Fusion. For *pUbi-FRT-STOP-FRT-mCD8::DQVD/A::QF2*, the FRT-STOP-FRT cassette
582 sequence was PCR amplified from *pJFRC201-10xUAS-FRT-STOP-FRT-myr::smGFP-HA*
583 (#63166; Addgene). The coding sequence of mCD8::DQVD/A was PCR-amplified from the
584 genomic DNA of *Caspase-Sensitive/Insensitive-Gal4* (Tang et al., 2015). The coding sequence
585 of QF2 was PCR amplified from the *pBPQUw* plasmid (Kashio et al., 2016). The three
586 fragments were ligated into *Eco*RI-digested *pUbi83* vector (a gift from D. Umetsu) using In-
587 Fusion. For *pQUAST-mNeonGreen*, the coding sequence of mNeonGreen was PCR-amplified
588 from *pAc5-V5::mNeonGreen* and ligated into the *Eco*RI-digested *pQUAST* (#24349, Addgene)
589 vector using In-Fusion. For *pUASz-FLPo*, the coding sequences of FLPo were PCR-amplified
590 from *pQUAST-FLPo* (#24357, Addgene) and ligated into the *Xho*I-digested *pUASz1.0* vector
591 using In-Fusion. For *pWALIUM20-Fas3G-shRNA*, the top and bottom oligonucleotides
592 including *mRNA* sequence specific to isoform G (5'-AATGAACCAAAGCAAGACAAA-3')
593 were annealed in annealing buffer (10 mM Tris-HCl, 0.1 M NaCl, 1 mM EDTA). The annealed
594 fragment was ligated into *Nhe*I/*Eco*RI-digested *pWALIUM20* (#1472, DGRC) vector using
595 DNA Ligation Kit <Mighty Mix> (#6023, TaKaRa).
596 All established plasmids were sequenced by Eurofins, Inc. The detailed plasmid DNA
597 sequences are available upon request. The established plasmids were injected into y^1, w^{67c23};
598 *P[CaryP]attP40* (*pUASz-3xFLAG::mNeonGreen*, *pUASz-Drice::myc::mNeonGreen*, *pUbi-*
599 *FRT-STOP-FRT-mCD8::DQVD/A::QF2* and *pWALIUM20-Fas3G-shRNA*) or y^1, w^{67c23};
600 *P[CaryP]attP2* (*pUASz-Fasciclin 3s::3xFLAG*, *pUASz-V5::TurboID* and *pUASz-*
601 *Caspase::V5::TurboID*) for PhiC31-mediated transgenesis (BestGene Inc.). Each red-eye-
602 positive transformant was isogenized. Integration of the attP landing site was confirmed using
603 genomic PCR.
604

605 ***Cell culture***

606 *Drosophila* S2 cells were grown at 25°C in Schneider's *Drosophila* medium (#21720001,
607 GIBCO) supplemented with 10% (v/v) heat-inactivated fetal bovine serum, 100 U/ml penicillin,
608 and 100 μg/ml streptomycin (#168-23191, WAKO). Cells were seeded in 24-well plates and
609 transfected with the desired plasmids using Effectene Transfection Reagent (#301427,
610 QIAGEN) following the manufacturer's protocol. Sixteen hours after transfection, the cells
611 were reseeded into CELL CULTURE DISH, PS, 35/10 MM (#627870, Grainer BIO-ONE) and
612 incubated for 24 h. Images were obtained using a Leica AF6000 DMI6000 B microscope (Leica
613 Microsystems). Images were analyzed and edited using Fiji software (NIH Image).

614 For the substrate cleavage assay, cells were seeded in 12-well plates and were
615 transfected with desired *pAc5-Fas3::3xFLAG* plasmids using Effectene Transfection Reagent
616 following the manufacturer's protocol. After 40 h of incubation, the cells were treated with 10
617 μg/mL cycloheximide (CHX, #C7698, Sigma) for apoptosis induction. After 6 h of incubation,
618 cells were collected using RIPA buffer supplemented with cOmplete ULTRA EDTA-free
619 protease inhibitor cocktail depending on the cell status. For apoptotic cell lysate collection, cells
620 were resuspended by pipetting and were collected into a 1.5 mL tube. The cells were then
621 centrifuged at 800 ×g, 4 °C for 5 min, resuspended in PBS, and centrifuged again using the same
622 parameters. The cell pellets were then lysed with 100 μL RIPA buffer. For the other
623 experimental conditions, the cells were washed thrice with PBS and directly lysed on the plate
624 with 100 μL RIPA buffer. The supernatants were collected and snap-frozen in liquid nitrogen.
625 Protein concentrations were determined using the BCA assay following the manufacturer's
626 protocol. The samples were mixed with 6x Laemmli buffer, boiled at 95°C for 5 min, and then
627 subjected to western blot analysis.

628 For the validation of Fas3G-shRNA, cells were seeded in 12-well plates and were co-
629 transfected with *pActin-Gal4,* desired *pUASz-Fas3::3xFLAG* and *pWALIUM20-empty* or

630 *pWALIUM20-Fas3G-shRNA* plasmids using Effectene Transfection Reagent following the
631 manufacturer's protocol. After 40 h of incubation, the cells were washed thrice with PBS and
632 directly lysed on the plate with 100 μL RIPA buffer. The supernatants were collected and snap-
633 frozen in liquid nitrogen. Protein concentrations were determined using the BCA assay
634 following the manufacturer's protocol. The samples were mixed with 6x Laemmli buffer,
635 boiled at 95°C for 5 min, and then subjected to western blot analysis.
636
637 ***Aging experiment***
638 Adult male flies were raised in vials containing 15 fly/vial, and incubated at 29°C, 65%
639 humidity with 12 h/12 h light/dark cycle. The flies were transferred every 2–4 days to vials
640 containing fresh food.
641
642 ***Two choice preference assay***
643 Newly eclosed adult male flies were raised in vials containing 25 fly/vial, and incubated at 29°C,
644 65% humidity with 12 h/12 h light/dark cycle. The flies were transferred every 2–4 days to vials
645 containing fresh food for 1 week. The 1-week-old young flies were starved in MilliQ (MQ)
646 water for 4 h or 16 h prior to the assay in constant dark condition. About 75 flies were put in
647 1000-mL glass beaker, which contained two standards bottles (traps) filled with 500 μl 1% or
648 25% apple cider vinegar (ACV; Mizkan) and 500 μl MQ water. The bottles were then covered
649 with sponge plugs containing pipette tips. The pipette tip was cut to increase the size of the
650 opening such that only one fly could climb into the bottle at a time. The glass beaker was
651 covered with a mesh fabric (Figure 6A). The beakers were set in an incubator at 29°C for 2 h
652 for the assay in constant dark condition. The experiments were evaluated only if at least one of
653 the tested flies entered either of 2 bottles. The preference index equaled the number of flies in
654 the ACV minus the number of flies in the MQ water, divided by the number of total live flies

655 in both inside and outside of the bottles, and multiplied by 100. Values greater than zero indicate
656 a preference for ACV and values less than zero indicate aversion. We repeated the same
657 experiment with different sets of flies and the number of times is indicated by N.
658
659 ***Statistical analysis***
660 Statistical analyses were performed using the GraphPad Prism 8 software (MDF). Data are
661 shown as the means ± standard error of the mean. *P*-values were calculated using a one-way
662 analysis of variance (ANOVA) with Bonferroni correction (Figure 4B for selected pairs, Figure
663 4D for every pair). *P*-values were calculated using the chi-square test with Bonferroni's
664 correction, with mNeonGreen as a control (Figure 4G), LacZ-RNAi as a control (Figure 4–
665 figure supplement 1D), and mNeonGreen and Fas3G as controls (Figure 4I, 5D). *P*-value was
666 calculated using unpaired *t*-test (Figure 6B). *P*-values were calculated using one-way ANOVA
667 with Dunnett's multiple comparison test (Figure 6C, mNeonGreen and Fas3G as controls). NS:
668 $P > 0.05$, †: < 0.05.
669

670 **Acknowledgments**

671 We would like to thank Dr. D. Umetsu, Dr. H. Kazama, Addgene and *Drosophila* Genomics
672 Resource Center for providing plasmids, Dr. Y. Nitta, Dr. A. Sugie, and Dr. T. Ichinose for
673 helpful discussions, and the Bloomington *Drosophila* Stock Center, Vienna Drosophila
674 Resource Center and Kyoto Stock Center for providing the fly strains. We thank Dr. S.
675 Hirayama, Dr. S. Murata, and the one-stop sharing faculty center for future drug discovery at
676 the Graduate School of Pharmaceutical Sciences, University of Tokyo, for the LC-MS/MS
677 analysis. We thank Miura's lab members for their technical assistance and discussions; in
678 particular, K. Takenaga for preparing the fly food, and R. Takamoto for experimental support.
679 The MASCaT was established by MASaya Muramoto with critical advice from Shu MASuda
680 at MASayuki Miura lab. We would like to thank *Editage* (www.editage.com) for English
681 language editing of this manuscript. This work was supported by grants from the Ministry of
682 Education, Culture, Sports, Science, and Technology of Japan (KAKENHI Grant Numbers
683 19K16137, 21K15080, 22H05586, and 23K05747 to N.S. and 21H04774, 21K19206,
684 23H04766, and 24H00567 to M.Mi.), the Japan Agency for Medical Research and
685 Development (AMED; Grant number JP21gm5010001 to M.Mi.), and grants from the Takeda
686 Science Foundation and Sumitomo Foundation to N.S.

687

688 **Author Contributions**

689 M.Mi. and N.S. designed the study; M.Mu., N.H. and N.S. conducted all the experiments and
690 analyzed all the data; M.O. and T.C. supervised the two choice preference assay; M.Mu., N.H.,
691 M.Mi. and N.S. wrote the manuscript.

692

693 **Conflict of Interests**

694 The authors declare that they have no conflict of interest.

References

Amcheslavsky A, Wang S, Fogarty CE, Lindblad JL, Fan Y, Bergmann A. 2018. Plasma membrane localization of apoptotic caspases for non-apoptotic functions. *Dev Cell* **45**:450-464.e3.

Aram L, Yacobi-Sharon K, Arama E. 2017. CDPs: caspase-dependent non-lethal cellular processes. *Cell Death Differ* **24**:1307–1310.

Boucher D, Blais V, Denault J-B. 2012. Caspase-7 uses an exosite to promote poly(ADP ribose) polymerase 1 proteolysis. *Proc Natl Acad Sci U S A* **109**:5669–5674.

Branon TC, Bosch JA, Sanchez AD, Udeshi ND, Svinkina T, Carr SA, Feldman JL, Perrimon N, Ting AY. 2018. Efficient proximity labeling in living cells and organisms with TurboID. *Nat Biotechnol* **36**:880–887.

Campbell DS, Okamoto H. 2013. Local caspase activation interacts with Slit-Robo signaling to restrict axonal arborization. *J Cell Biol* **203**:657–672.

Cheriyamkunnel SJ, Rose S, Jacob PF, Blackburn LA, Glasgow S, Moorse J, Winstanley M, Moynihan PJ, Waddell S, Rezaval C. 2021. A neuronal mechanism controlling the choice between feeding and sexual behaviors in Drosophila. *Curr Biol* **31**:4231-4245.e4.

Chiba A, Snow P, Keshishian H, Hotta Y. 1995. Fasciclin III as a synaptic target recognition molecule in Drosophila. *Nature* **374**:166–168.

Chihara T, Kitabayashi A, Morimoto M, Takeuchi K-I, Masuyama K, Tonoki A, Davis RL, Wang JW, Miura M. 2014. Caspase inhibition in select olfactory neurons restores innate attraction behavior in aged Drosophila. *PLoS Genet* **10**:e1004437.

D'Brot A, Chen P, Vaishnav M, Yuan S, Akey CW, Abrams JM. 2013. Tango7 directs cellular remodeling by the Drosophila apoptosome. *Genes Dev* **27**:1650–1655.

Dehkordi MH, Munn RGK, Fearnhead HO. 2022. Non-canonical roles of apoptotic caspases in the nervous system. *Front Cell Dev Biol* **10**:840023.

DeLuca SZ, Spradling AC. 2018. Efficient expression of genes in the Drosophila germline using a UAS promoter free of interference by Hsp70 piRNAs. *Genetics* **209**:381–387.

Desroches A, Denault J-B. 2019. Caspase-7 uses RNA to enhance proteolysis of poly(ADP-ribose) polymerase 1 and other RNA-binding proteins. *Proc Natl Acad Sci U S A* **116**:21521–21528.

Ding AX, Sun G, Argaw YG, Wong JO, Easwaran S, Montell DJ. 2016. CasExpress reveals widespread and diverse patterns of cell survival of caspase-3 activation during development in vivo. *Elife* **5**. doi:10.7554/eLife.10936

Ditzel M, Broemer M, Tenev T, Bolduc C, Lee TV, Rigbolt KTG, Elliott R, Zvelebil M, Blagoev B, Bergmann A, Meier P. 2008. Inactivation of effector caspases through nondegradative polyubiquitylation. *Mol Cell* **32**:540–553.

Dorstyn L, Colussi PA, Quinn LM, Richardson H, Kumar S. 1999. DRONC, an ecdysone-inducible Drosophila caspase. *Proc Natl Acad Sci U S A* **96**:4307–4312.

Evans R, O'Neill M, Pritzel A, Antropova N, Senior A, Green T, Žídek A, Bates R, Blackwell S, Yim J, Ronneberger O, Bodenstein S, Zielinski M, Bridgland A, Potapenko A, Cowie A, Tunyasuvunakool K, Jain R, Clancy E, Kohli P, Jumper J, Hassabis D. 2021. Protein complex prediction with AlphaFold-Multimer. *bioRxiv*. doi:10.1101/2021.10.04.463034

González M, Martín-Ruíz I, Jiménez S, Pirone L, Barrio R, Sutherland JD. 2011. Generation of stable Drosophila cell lines using multicistronic vectors. *Sci Rep* **1**:75.

Green DR. 2019. The coming decade of cell death research: Five riddles. *Cell* **177**:1094–1107.

Gu Q, Jiao S, Duan K, Wang Y-X, Petralia RS, Li Z. 2021. The BAD-BAX-caspase-3 cascade modulates synaptic vesicle pools via autophagy. *J Neurosci* **41**:1174–1190.

Hay BA, Wassarman DA, Rubin GM. 1995. Drosophila homologs of baculovirus inhibitor of

apoptosis proteins function to block cell death. *Cell* **83**:1253–1262.
Huang DW, Sherman BT, Lempicki RA. 2009. Bioinformatics enrichment tools: paths toward the comprehensive functional analysis of large gene lists. *Nucleic Acids Res* **37**:1–13.
Julien O, Wells JA. 2017. Caspases and their substrates. *Cell Death Differ* **24**:1380–1389.
Kang Y, Neuman SD, Bashirullah A. 2017. Tango7 regulates cortical activity of caspases during reaper-triggered changes in tissue elasticity. *Nat Commun* **8**:603.
Kanuka H, Kuranaga E, Takemoto K, Hiratou T, Okano H, Miura M. 2005. Drosophila caspase transduces Shaggy/GSK-3beta kinase activity in neural precursor development. *EMBO J* **24**:3793–3806.
Karim MR, Endo K, Moore AW, Taniguchi H. 2014. Whole mount immunolabeling of olfactory receptor neurons in the Drosophila antenna. *J Vis Exp*. doi:10.3791/51245-v
Kashio S, Obata F, Zhang L, Katsuyama T, Chihara T, Miura M. 2016. Tissue nonautonomous effects of fat body methionine metabolism on imaginal disc repair in Drosophila. *Proc Natl Acad Sci U S A* **113**:1835–1840.
Kose H, Rose D, Zhu X, Chiba A. 1997. Homophilic synaptic target recognition mediated by immunoglobulin-like cell adhesion molecule Fasciclin III. *Development* **124**:4143–4152.
Kumar S. 2007. Caspase function in programmed cell death. *Cell Death Differ* **14**:32–43.
Kumar S, Dorstyn L, Lim Y. 2022. The role of caspases as executioners of apoptosis. *Biochem Soc Trans* **50**:33–45.
Lee TV, Fan Y, Wang S, Srivastava M, Broemer M, Meier P, Bergmann A. 2011. Drosophila IAP1-mediated ubiquitylation controls activation of the initiator caspase DRONC independent of protein degradation. *PLoS Genet* **7**:e1002261.
Li L, Ding Z, Pang T-L, Zhang B, Li C-H, Liang A-M, Wang Y-R, Zhou Y, Fan Y-J, Xu Y-Z. 2020. Defective minor spliceosomes induce SMA-associated phenotypes through sensitive intron-containing neural genes in Drosophila. *Nat Commun* **11**:5608.
Li Z, Jo J, Jia J-M, Lo S-C, Whitcomb DJ, Jiao S, Cho K, Sheng M. 2010. Caspase-3 activation via mitochondria is required for long-term depression and AMPA receptor internalization. *Cell* **141**:859–871.
Luck K, Kim D-K, Lambourne L, Spirohn K, Begg BE, Bian W, Brignall R, Cafarelli T, Campos-Laborie FJ, Charloteaux B, Choi D, Coté AG, Daley M, Deimling S, Desbuleux A, Dricot A, Gebbia M, Hardy MF, Kishore N, Knapp JJ, Kovács IA, Lemmens I, Mee MW, Mellor JC, Pollis C, Pons C, Richardson AD, Schlabach S, Teeking B, Yadav A, Babor M, Balcha D, Basha O, Bowman-Colin C, Chin S-F, Choi SG, Colabella C, Coppin G, D'Amata C, De Ridder D, De Rouck S, Duran-Frigola M, Ennajdaoui H, Goebels F, Goehring L, Gopal A, Haddad G, Hatchi E, Helmy M, Jacob Y, Kassa Y, Landini S, Li R, van Lieshout N, MacWilliams A, Markey D, Paulson JN, Rangarajan S, Rasla J, Rayhan A, Rolland T, San-Miguel A, Shen Y, Sheykhkarimli D, Sheynkman GM, Simonovsky E, Taşan M, Tejeda A, Tropepe V, Twizere J-C, Wang Y, Weatheritt RJ, Weile J, Xia Y, Yang X, Yeger-Lotem E, Zhong Q, Aloy P, Bader GD, De Las Rivas J, Gaudet S, Hao T, Rak J, Tavernier J, Hill DE, Vidal M, Roth FP, Calderwood MA. 2020. A reference map of the human binary protein interactome. *Nature* **580**:402–408.
Mirdita M, Schütze K, Moriwaki Y, Heo L, Ovchinnikov S, Steinegger M. 2022. ColabFold: making protein folding accessible to all. *Nat Methods* **19**:679–682.
Mukherjee A, Williams DW. 2017. More alive than dead: non-apoptotic roles for caspases in neuronal development, plasticity and disease. *Cell Death Differ* **24**:1411–1421.
Nakajima Y-I, Kuranaga E. 2017. Caspase-dependent non-apoptotic processes in development. *Cell Death Differ* **24**:1422–1430.
Ohsawa S, Hamada S, Kuida K, Yoshida H, Igaki T, Miura M. 2010. Maturation of the olfactory

794 sensory neurons by Apaf-1/caspase-9-mediated caspase activity. *Proc Natl Acad Sci U*
795 *S A* **107**:13366–13371.
796 Okuda S, Watanabe Y, Moriya Y, Kawano S, Yamamoto T, Matsumoto M, Takami T,
797 Kobayashi D, Araki N, Yoshizawa AC, Tabata T, Sugiyama N, Goto S, Ishihama Y.
798 2017. jPOSTrepo: an international standard data repository for proteomes. *Nucleic*
799 *Acids Res* **45**:D1107–D1111.
800 Orme MH, Liccardi G, Moderau N, Feltham R, Wicky-John S, Tenev T, Aram L, Wilson R,
801 Bianchi K, Morris O, Monteiro Domingues C, Robertson D, Tare M, Wepf A, Williams
802 D, Bergmann A, Gstaiger M, Arama E, Ribeiro PS, Meier P. 2016. The unconventional
803 myosin CRINKLED and its mammalian orthologue MYO7A regulate caspases in their
804 signalling roles. *Nat Commun* **7**:10972.
805 Qin W, Cho KF, Cavanagh PE, Ting AY. 2021. Deciphering molecular interactions by
806 proximity labeling. *Nat Methods* **18**:133–143.
807 Semmelhack JL, Wang JW. 2009. Select Drosophila glomeruli mediate innate olfactory
808 attraction and aversion. *Nature* **459**:218–223.
809 Shinoda N, Hanawa N, Chihara T, Koto A, Miura M. 2019. Dronc-independent basal
810 executioner caspase activity sustains Drosophila imaginal tissue growth. *Proc Natl Acad*
811 *Sci U S A* **116**:20539–20544.
812 Shinoda N, Horikoshi M, Taira Y, Muramoto M, Hirayama S, Murata S, Miura M. 2023.
813 Caspase cleaves Drosophila BubR1 to modulate spindle assembly checkpoint function
814 and lifespan of the organism. *FEBS J* **290**:4200–4223.
815 Shinoda N, Miura M. 2024. Exploring caspase-dependent non-lethal cellular processes using
816 Drosophila. *Front Cell Death* **3**:1472108.
817 Takemoto K, Nagai T, Miyawaki A, Miura M. 2003. Spatio-temporal activation of caspase
818 revealed by indicator that is insensitive to environmental effects. *J Cell Biol* **160**:235–
819 243.
820 Tang HL, Tang HM, Fung MC, Hardwick JM. 2015. In vivo CaspaseTracker biosensor system
821 for detecting anastasis and non-apoptotic caspase activity. *Sci Rep* **5**:9015.
822 Valente P, Lignani G, Medrihan L, Bosco F, Contestabile A, Lippiello P, Ferrea E, Schachner
823 M, Benfenati F, Giovedì S, Baldelli P. 2016. Cell adhesion molecule L1 contributes to
824 neuronal excitability regulating the function of voltage-gated Na+ channels. *J Cell Sci*
825 **129**:1878–1891.
826 Verghese S, Bedi S, Kango-Singh M. 2012. Hippo signalling controls Dronc activity to regulate
827 organ size in Drosophila. *Cell Death Differ* **19**:1664–1676.
828 Walsh JG, Cullen SP, Sheridan C, Lüthi AU, Gerner C, Martin SJ. 2008. Executioner caspase-
829 3 and caspase-7 are functionally distinct proteases. *Proc Natl Acad Sci U S A*
830 **105**:12815–12819.
831 Westphal D, Sytnyk V, Schachner M, Leshchyns'ka I. 2010. Clustering of the neural cell
832 adhesion molecule (NCAM) at the neuronal cell surface induces caspase-8- and -3-
833 dependent changes of the spectrin meshwork required for NCAM-mediated neurite
834 outgrowth. *J Biol Chem* **285**:42046–42057.
835 Williams DW, Kondo S, Krzyzanowska A, Hiromi Y, Truman JW. 2006. Local caspase activity
836 directs engulfment of dendrites during pruning. *Nat Neurosci* **9**:1234–1236.
837

838 **Figures & Figure Legends**

839 **Figure 1**

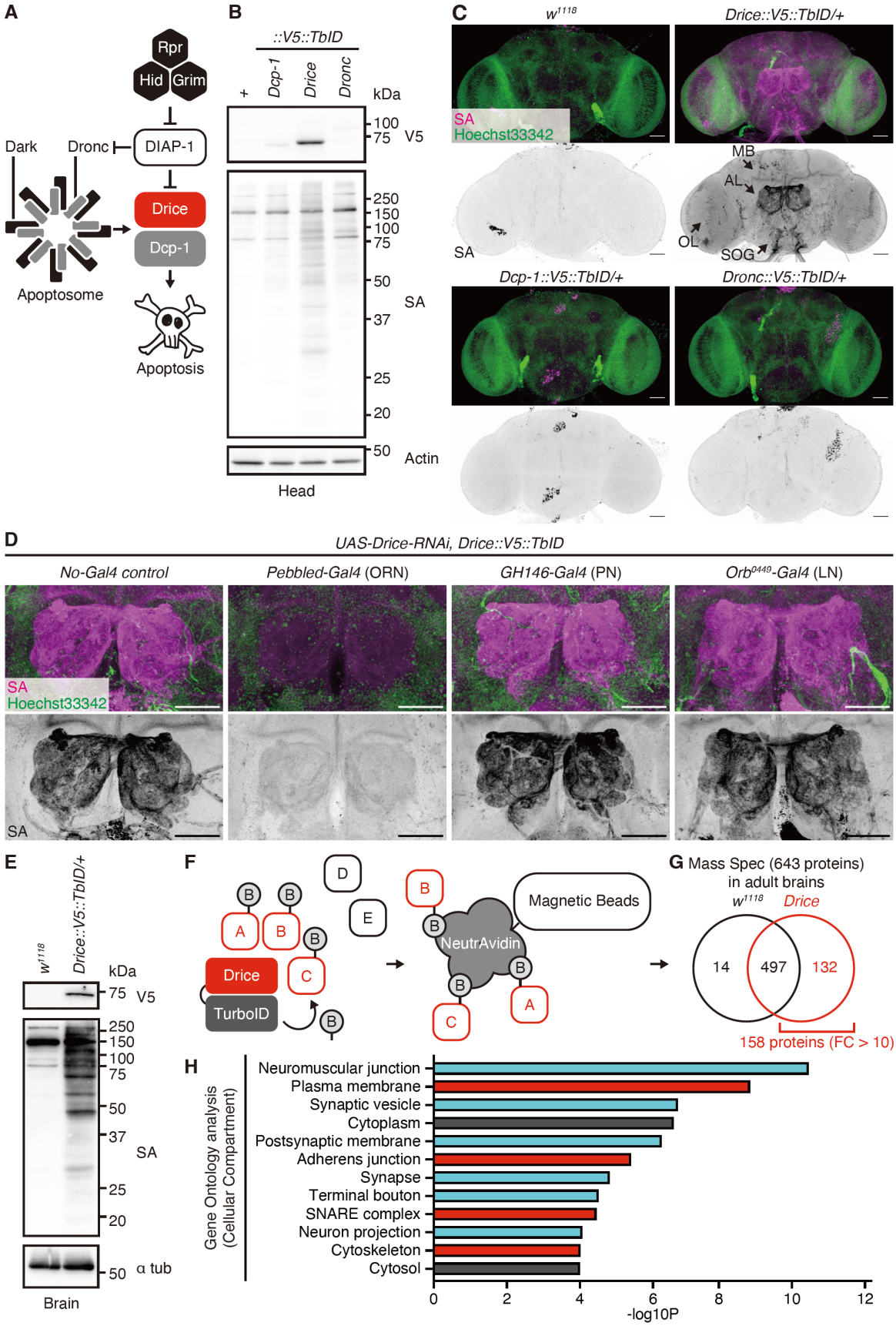

840

841 **Figure 1. Expression patterns and proximal proteins of Drice in the adult brain.**

842 **(A)** Schematic diagram of *Drosophila* apoptosis signaling.

843 **(B)** Western blot of expression of C-terminally V5::TurboID knocked-in tagged caspases in
844 adult male heads. Biotinylated proteins are detected by streptavidin (SA).

845 **(C)** Representative images of adult male brains. Expression patterns of each C-terminally
846 V5::TurboID knocked-in tagged caspase are visualized using SA (magenta). Nuclei are
847 visualized by Hoechst33342 (green). Arrows indicate the mushroom body (MB), antennal
848 lobe (AL), optic lobe (OL), and suboesophageal ganglion (SOG), respectively. Scale bar:
849 50 μm.

850 **(D)** Representative images of ALs in the adult male brains. Expression patterns of Drice are
851 visualized using SA (magenta). Nuclei are visualized by Hoechst33342 (green). Scale bar:
852 50 μm.

853 **(E)** Western blot of biotinylated proteins labelled by Drice::V5::TurboID extracted from adult
854 male brains. Biotinylated proteins are detected by streptavidin (SA).

855 **(F)** Schematic diagram of the TurboID-mediated identification of proximal proteins. Drice
856 proximal proteins are promiscuously labeled *in vivo* with the administration of biotin. Then,
857 biotinylated proteins are purified using NeutrAvidin magnetic beads and are subsequently
858 analyzed by mass spectrometry.

859 **(G)** A summary of mass spectrometry analysis of proteins of the adult male brains. Among 643
860 proteins identified, 158 proteins were detected as highly specific proteins to
861 *Drice::V5::TurboID* flies compared to wild-type flies (FC (*Drice::V5::TurboID*/w^{1118}) >
862 10).

863 **(H)** Gene Ontology analysis (Cellular Compartment) of 158 Drice proximal proteins (FC
864 (*Drice::V5::TurboID*/w^{1118}) > 10). Cyan: neuronal-related fraction, Red: membrane
865 fraction.

866

867 **Figure 1–figure supplement 1**

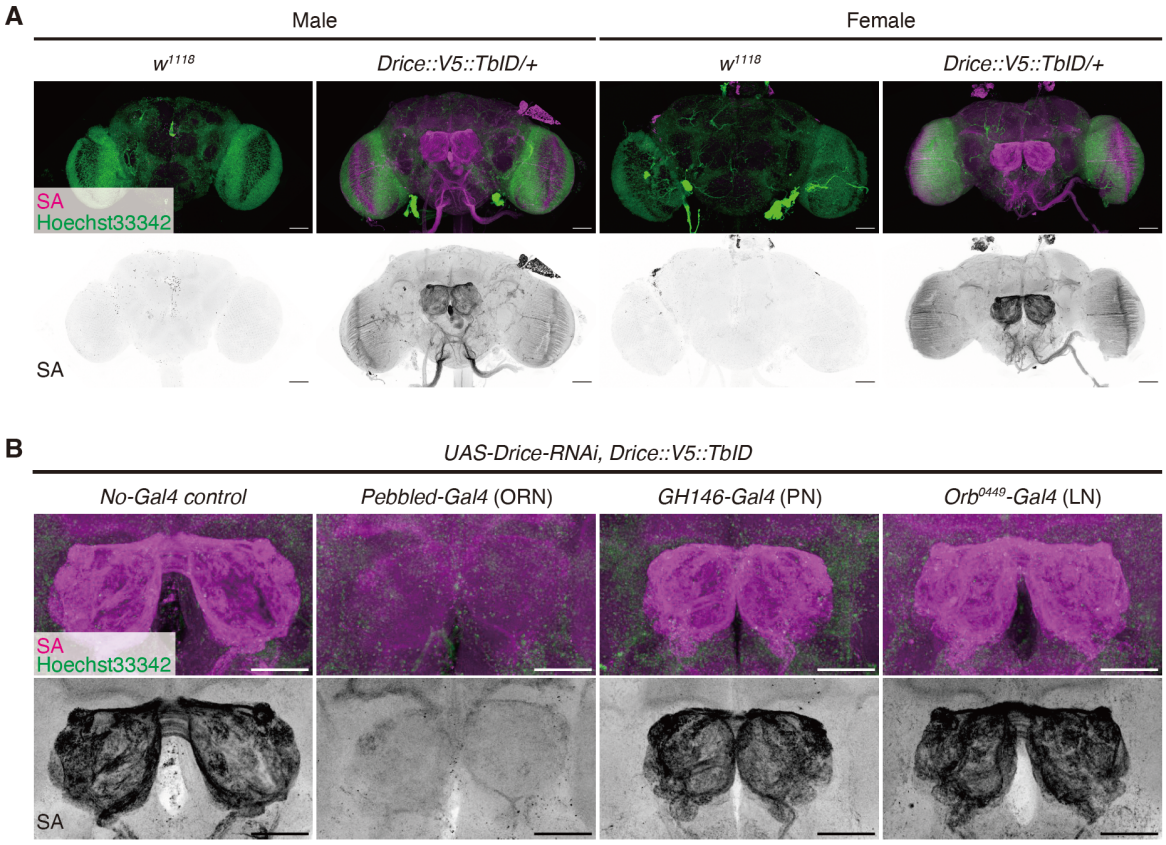

868

869 **Figure 1–figure supplement 1. Expression patterns of Drice in the adult brain in males**
870 **and females.**

871 **(A)** Representative images of adult male and female brains. Expression patterns of C-terminally
872 V5::TurboID knocked-in tagged Drice are visualized using Streptavidin (SA, magenta).
873 Nuclei are visualized by Hoechst33342 (green). Scale bar: 50 μm.

874 **(B)** Representative images of antennal lobes in the adult female brains. Expression patterns of
875 Drice are visualized using SA (magenta). Nuclei are visualized by Hoechst33342 (green).
876 Scale bar: 50 μm.

877

878 **Figure 2**

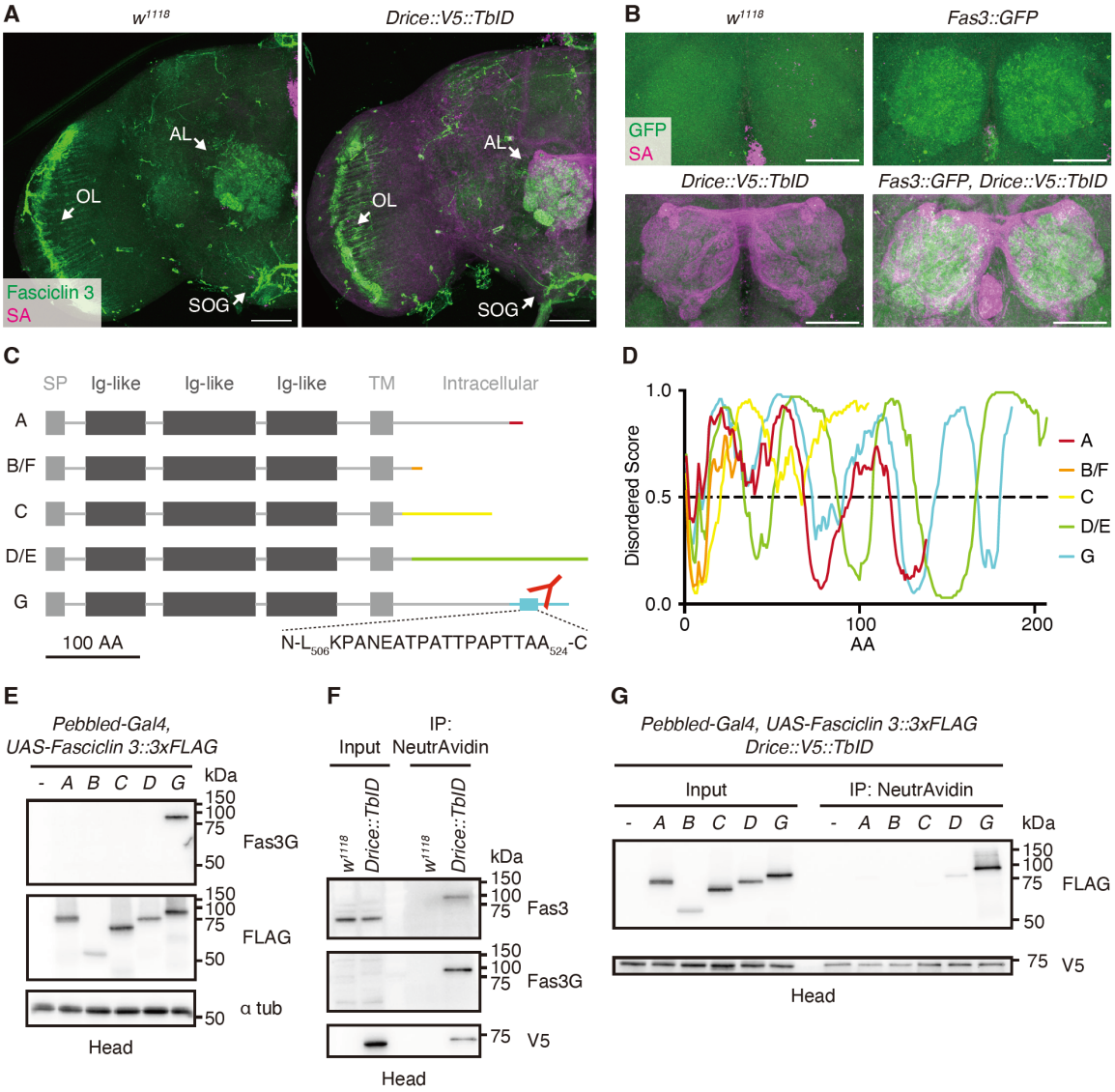

879

880 **Figure 2. A specific isoform of Fasciclin 3 is in proximity to Drice.**

881 **(A)** Representative expression patterns of C-terminally V5::TurboID knocked-in tagged Drice
882 (Streptavidin (SA); magenta) and Fasciclin 3 (Fas3, anti-Fasciclin 3 antibody staining;
883 green) in the adult male brains. Arrows indicate the antennal lobe (AL), optic lobe (OL),
884 and suboesophageal ganglion (SOG), respectively. Scale bar: 50 μm.

885 **(B)** Representative expression patterns of C-terminally V5::TurboID knocked-in tagged Drice
886 (SA; magenta) and Fas3 (anti-GFP antibody staining; green) in the antennal lobes (ALs) of
887 the adult male brains. Scale bar: 50 μm.

888 **(C)** Schematic protein structures of Fas3 isoforms. Intracellular regions differ from each other.
889 A peptide region used to raise anti-Fas3G antibody is shown. Signal peptides (SPs),
890 immunoglobulin-like (Ig-like) domains, and transmembrane (TM) domains are shown in
891 boxes.

892 **(D)** IDR predictions of intracellular regions of each protein isoform. Regions wherein the score
893 is more than 0.5 are predicted to be disordered.
894 **(E)** Western blot of proteins extracted from adult heads overexpressing each *3xFLAG-tagged*
895 *Fas3 isoform*. Anti-Fas3G antibody specifically detects Fas3 isoform G.
896 **(F)** Western blot of endogenous Fas3 expressed in adult male heads. Drice proximal proteins
897 biotinylated by C-terminally knocked-in tagged V5::TurboID are purified using
898 NeturAvidin
899 **(G)** Western blot of 3xFLAG-tagged Fas3 isoforms overexpressed in adult head. Drice
900 proximal proteins biotinylated by C-terminally knocked-in tagged V5::TurboID are
901 purified using NeturAvidin.
902

903 **Figure 2–figure supplement 1**

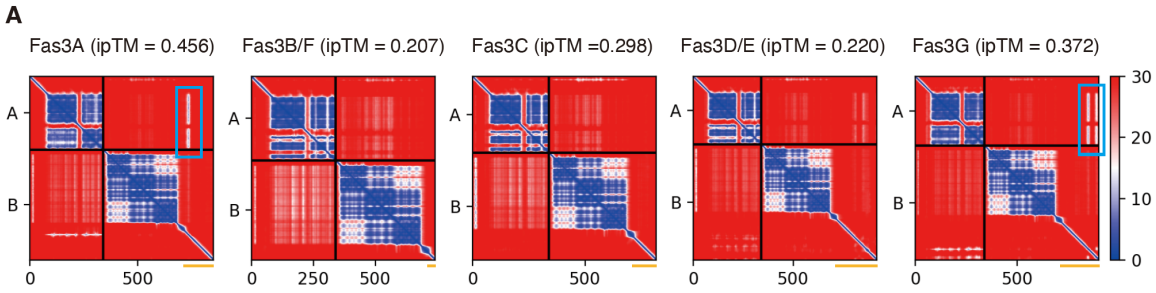

904

905 **Figure 2–figure supplement 1. Predicted protein complexes of Drice and each Fas3**
906 **isoform**

907 **(A)** Predicted aligned error (PAE) plots of protein complex of Drice and each Fasciclin 3 (Fas3)
908 isoform generated by AlphaFold2-Multimer. In Y axis, A represents Drice and B represents
909 each Fas3 isoform. Numbers in X axis represent amino acid position. The intracellular
910 region of each Fas3 isoform is represented by the orange bar. Potential interaction sites
911 predicted by low PAE scores in Drice-Fas3A/G are highlighted by blue rectangles.

912

913 **Figure 2–figure supplement 2**

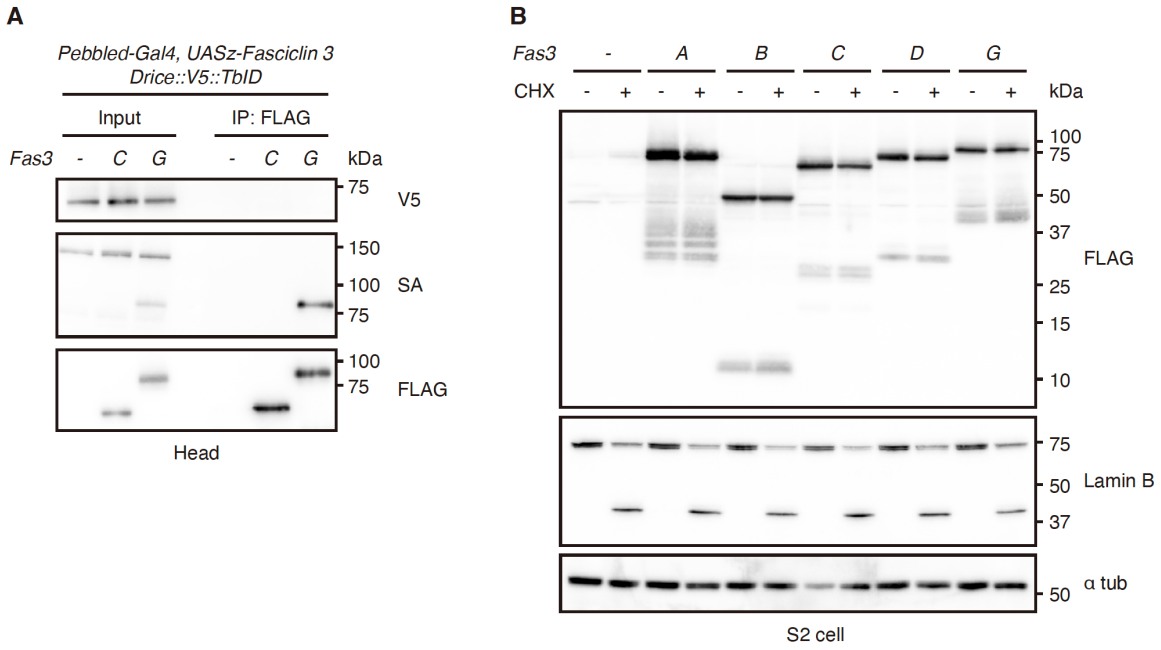

914

915 **Figure 2–figure supplement 2. Biochemical property of Fas3s with caspases.**

916 **(A)** Co-immunoprecipitation of 3xFLAG-tagged Fasciclin 3s (Fas3s) with V5-tagged Drice
917 extracted from adult male heads. 3xFLAG-tagged Fas3s are immunoprecipitated using an
918 anti-FLAG antibody. Biotinylated proteins labelled by Drice::V5::TurboID are detected by
919 streptavidin (SA).

920 **(B)** Western blot for 3xFLAG-tagged Fas3s expressed in *Drosophila* S2 cells. Apoptosis was
921 induced by treating *Drosophila* S2 cells with cycloheximide (CHX). Induction of caspase
922 activation is confirmed by the cleavage of endogenous Lamin B.

923

924 **Figure 3**

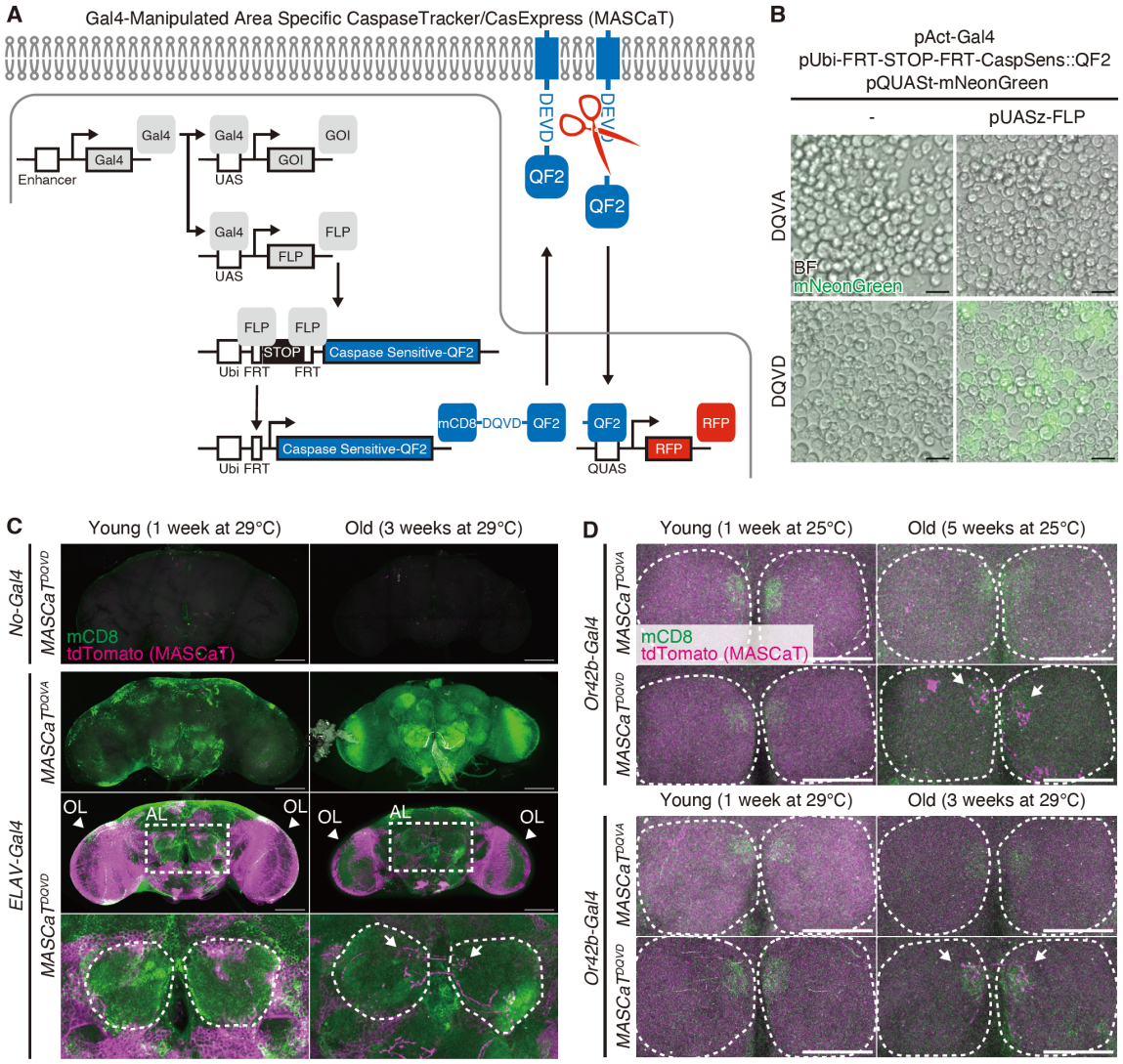

925

926 **Figure 3. A Gal4-Manipulated Area Specific CaspaseTracker/CasExpress (MASCaT).**

927 **(A)** A schematic diagram of MASCaT expressed using the Gal4/UAS system with FLP-
928 mediated recombination. Caspase sensitive-QF2 is activated by caspase-mediated cleavage
929 at the plasma membrane. Cleaved QF2 translocates to the nucleus to induce reporter protein
930 expression downstream of *QUAS* sequence.

931 **(B)** Representative images of *Drosophila* S2 cells expressing caspase sensitive-QF2 probes by
932 the Gal4/UAS system with FLP-mediated recombination. Scale bar: 20 µm.

933 **(C)** Representative images of adult male brains of young (1 week old) and old (3 weeks old)
934 flies raised at 29°C expressing MASCaT probe (mCD8; green). Caspase activation is
935 visualized by MASCaT-induced tdTomato (magenta) expression. Arrowheads indicate
936 optic lobes (OLs). Magnified images (white rectangle) show antennal lobes (ALs; white
937 circles). Arrows indicate age-dependent caspase activation at the ALs. Scale bar: 100 µm.

938 **(D)** Representative images of adult male brains of young (1 week old raised at 25℃ or 29℃)
939 and old (5 weeks old raised at 25℃ or 3 weeks old raised at 29℃) expressing MASCaT
940 probe (mCD8; green). Caspase activation is visualized by MASCaT-induced tdTomato
941 (magenta) expression. White circles show ALs. Arrows indicate age-dependent caspase
942 activation at the ALs. Scale bar: 50 µm.
943

944 **Figure 3–figure supplement 1**

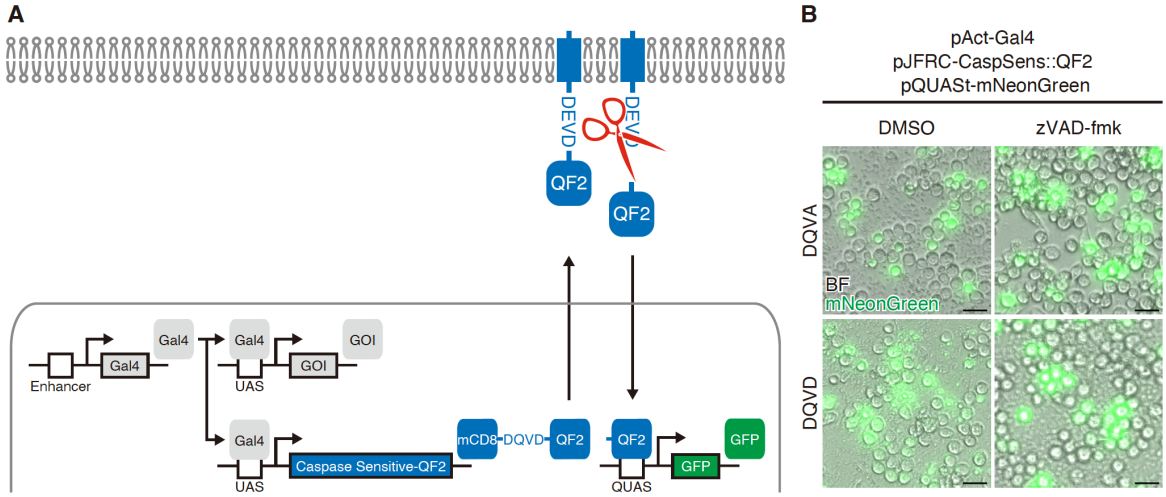

945

946 **Figure 3–figure supplement 1. Overexpression of *mCD8::DQVD::QF2* probes in**
947 ***Drosophila* S2 cells.**

948 **(A)** A schematic diagram of MASCaT expressed directly using the Gal4/UAS system. Caspase
949 sensitive-QF2 is activated by caspase-mediated cleavage at the plasma membrane. In theory,
950 only cleaved QF2 translocates to the nucleus to induce reporter protein expression
951 downstream of *QUAS* sequence.

952 **(B)** Representative images of *Drosophila* S2 cells expressing caspase sensitive-QF2 probes
953 directly by the Gal4/UAS system. A pan-caspase inhibitior, zVAD-fmk, is treated to inhibit
954 caspase activity. Scale bar: 20 μm.

955

956 **Figure 4**

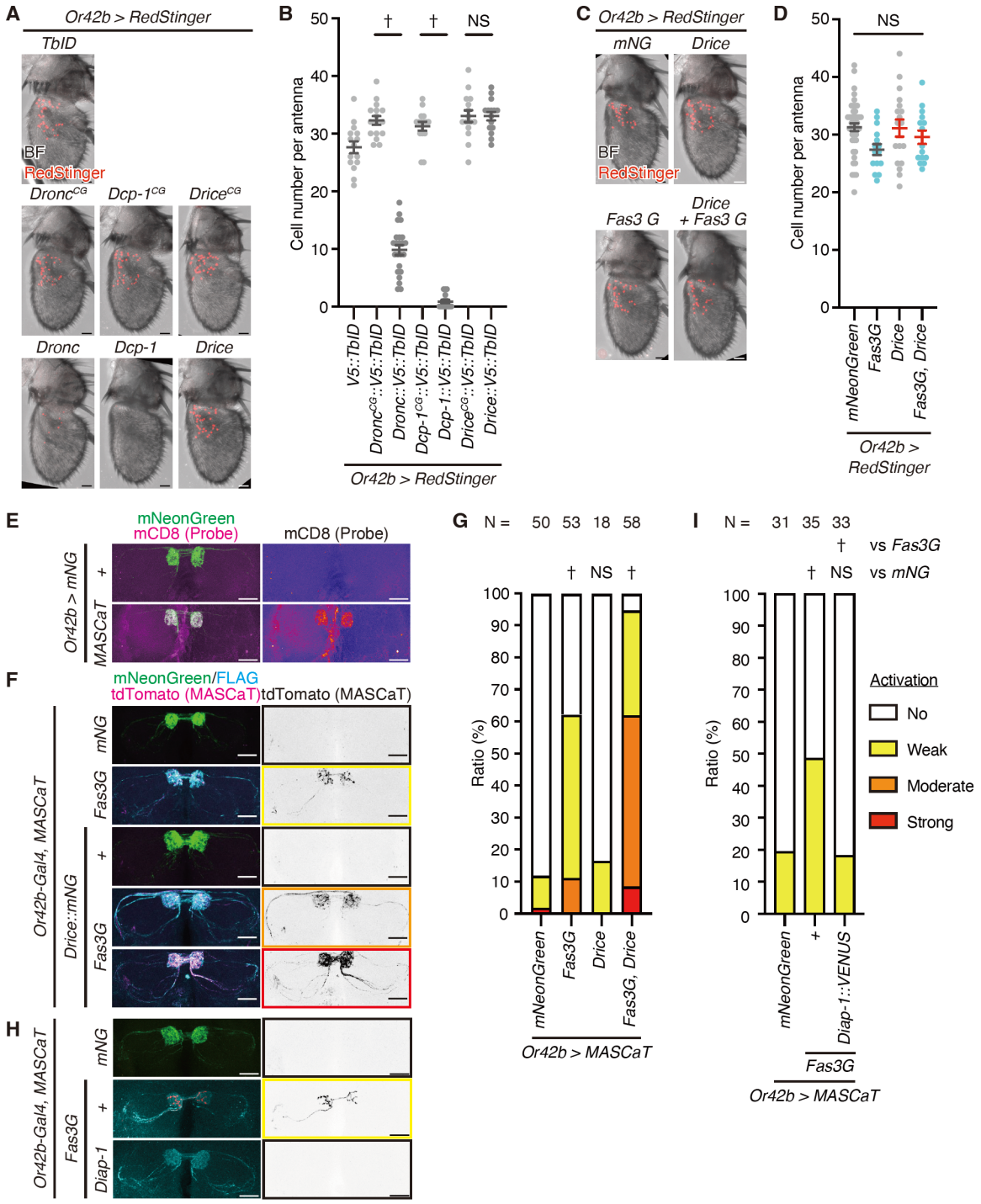

957

958 **Figure 4. *Fasciclin 3 isoform G* overexpression enhances non-lethal caspase activation.**

959 **(A)** Representative images of the adult male antennae of 1 weeks old flies raised at 29°C. Cell
960 bodies are visualized using RedStinger (red). Scale bar: 20 µm.

961 **(B)** Quantification of cell number of (A). Data are presented as mean ± SEM. *P*-values were
962 calculated using one-way analysis of variance (ANOVA) with Bonferroni's correction for
963 selected pairs. NS: $P > 0.05$, †: $P < 0.05$. Sample sizes: *V5::TbID* (N = 15),

964 *Dronc^{CG}::V5::TbID* (N = 16), *Dronc::V5::TbID* (N = 23), *Dcp-1^{CG}::V5::TbID* (N = 15),
965 *Dcp-1::V5::TbID* (N = 16), *Drice^{CG}::V5::TbID* (N = 15), *Drice::V5::TbID* (N = 15).
966 **(C)** Representative images of the adult male antennae of 1 week old flies raised at 29°C. Cell
967 bodies are visualized using RedStinger (red). Scale bar: 20 µm.
968 **(D)** Quantification of cell number of (C). Data are presented as mean ± SEM. Light blue dots
969 represent *Fas3G* overexpression conditions while red bars represent *Drice* overexpression
970 conditions. *P*-values were calculated using one-way ANOVA with Bonferroni's correction
971 for every pair. NS: $P > 0.05$. Sample sizes: *mNeonGreen* (N = 44), *Fasciclin 3 isoform G*
972 (*Fas3G*; N = 15), *Drice* (N = 18), *Fas3G* + *Drice* (N = 15).
973 **(E)** Representative images of the antennal lobes (ALs) of male brains of 1 week old flies raised
974 at 29°C expressing MASCaT probe (mCD8; magenta). Expression of the probes are
975 restricted to the *Or42b-Gal4* positive (mNeonGreen; green) regions. Scale bar: 30 µm.
976 **(F)** Representative images of the ALs of brains of 1 week old flies raised at 29°C with caspase
977 activation visualized by MASCaT-induced tdTomato (magenta) expression. Expression of
978 mNeonGreen (green) or 3xFLAG-tagged Fas3G (cyan) are simultaneously visualized.
979 Scale bar: 30 µm.
980 **(G)** Quantifications of caspase activity detected by MASCaT of (F). *P*-values were calculated
981 using chi-square test with Bonferroni's correction using mNeonGreen as control. NS: $P >$
982 0.05, †: $P < 0.05$. Sample sizes are shown in the graph.
983 **(H)** Representative images of the ALs of brains of 1 week old flies raised at 29°C with caspase
984 activation visualized by MASCaT-induced tdTomato (magenta) expression. Expression of
985 mNeonGreen (green) or 3xFLAG-tagged Fas3G (cyan) are simultaneously visualized.
986 Scale bar: 30 µm.
987 **(I)** Quantifications of caspase activity detected by MASCaT of (H). *P*-values were calculated
988 using chi-square test with Bonferroni's correction using mNeonGreen and Fas3G as
989 controls, respectively. NS: $P > 0.05$, †: $P < 0.05$. Sample sizes are shown in the graph.
990

991 **Figure 4–figure supplement 1**

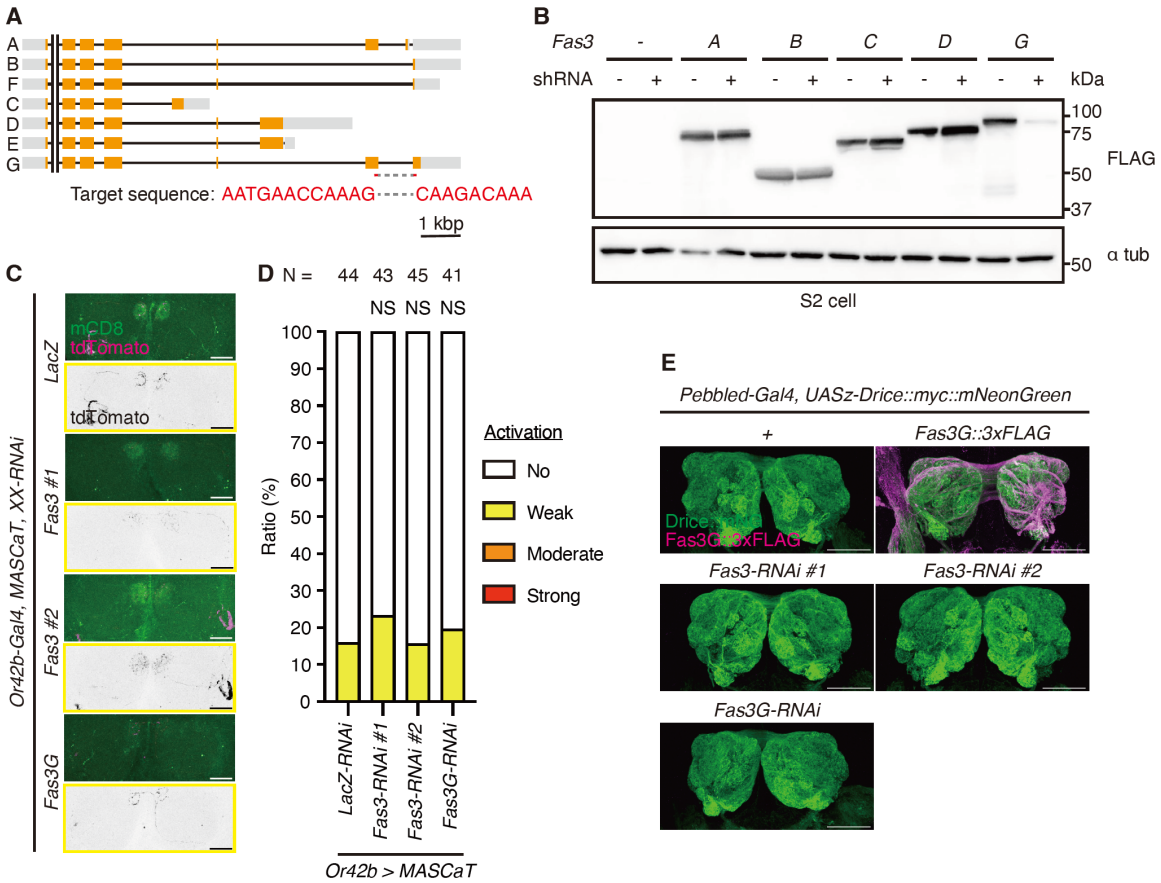

992

993 **Figure 4–figure supplement 1. Loss of function analysis of Fas3G.**

994 **(A)** Gene structure of Fasciclin 3 (Fas3). CDS (orange) and UTR (grey) are shown in boxes.
995 Target sequence of Fas3G-shRNA is shown in red.

996 **(B)** Western blot for 3xFLAG-tagged Fas3s expressed in *Drosophila* S2 cells with Fas3G-
997 shRNA.

998 **(C)** Representative images of the antennal lobes (ALs) of brains of 1 week old flies raised at
999 29°C with caspase activation visualized by MASCaT probe (mCD8; green)-induced
1000 tdTomato (magenta) expression. Scale bar: 30 µm.

1001 **(D)** Quantifications of caspase activity detected by MASCaT of (C). *P*-values were calculated
1002 using chi-square test with Bonferroni's correction using *LacZ-RNAi* as control. NS: $P >$
1003 0.05. Sample sizes are shown in the graph.

1004 **(E)** Representative images of the ALs of brains of 1 week old flies expressing mNeonGreen-
1005 tagged Drice (green) and 3xFLAG-tagged Fas3G (magenta). Scale bar: 50 µm.

1006

1007 **Figure 5**

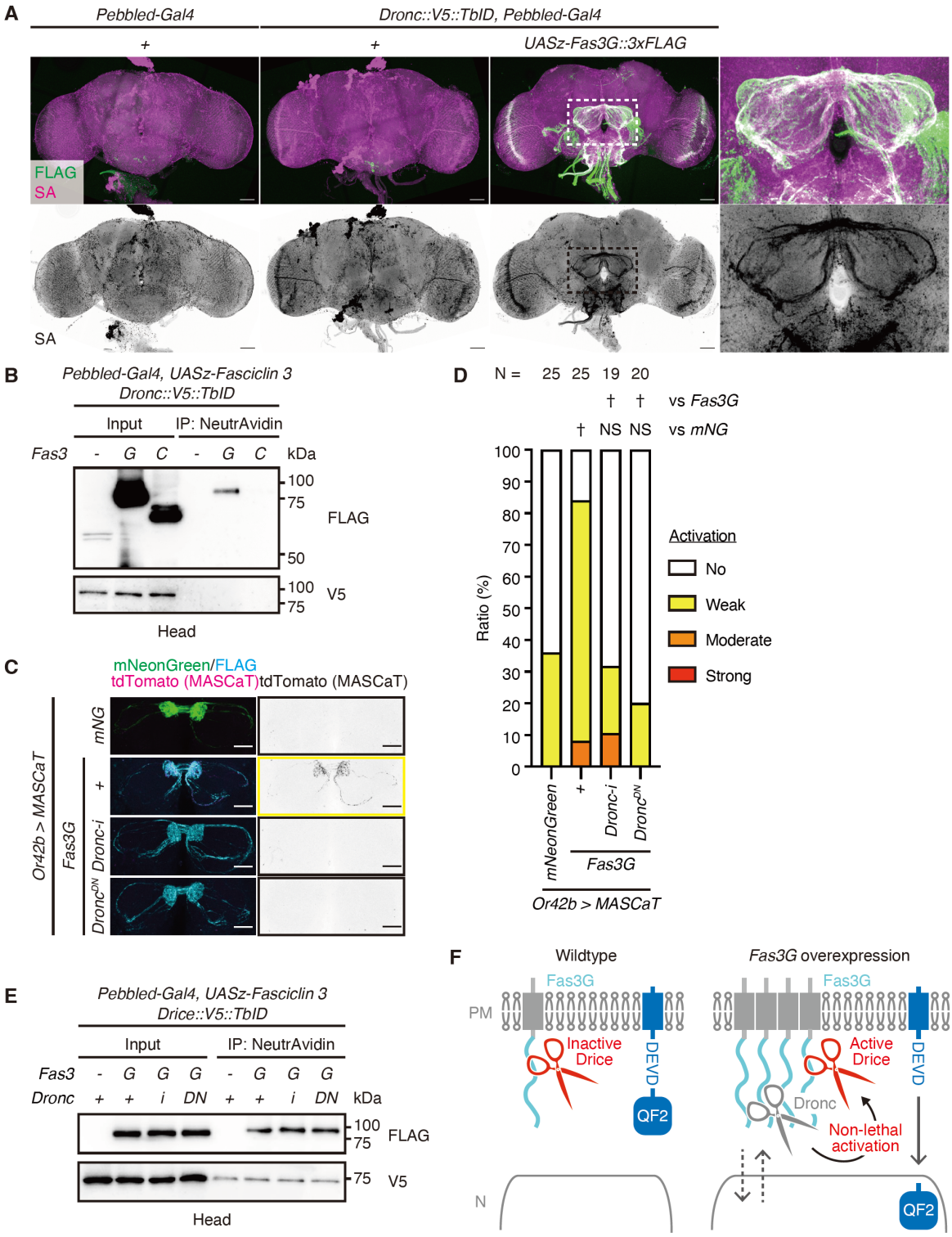

1008

1009 **Figure 5. *Fasciclin 3 isoform G* overexpression enhances non-lethal caspase activation in**

1010 **a Dronc-dependent manner.**

1011 **(A)** Representative images of adult male brains. Expression patterns of C-terminally

1012 V5::TurboID knocked-in tagged Dronc are visualized using Streptavidin (SA; magenta)

1013 with or without the expression of 3xFLAG-tagged Fasciclin isoform G (Fas3G; green).
1014 Magnified images (white rectangle) show antennal lobes (ALs). Scale bar: 50 μm.
1015 **(B)** Western blot of adult male heads. Dronc proximal proteins biotinylated by C-terminally
1016 knocked-in tagged V5::TurboID are purified using NeturAvidin.
1017 **(C)** Representative images of the AL of brains of 1 week old flies raised at 29°C with caspase
1018 activation visualized by MASCaT-induced tdTomato (magenta) expression. Expression
1019 of mNeonGreen (green) or 3xFLAG-tagged Fas3G (cyan) are simultaneously visualized.
1020 Scale bar: 30 μm.
1021 **(D)** Quantifications of caspase activity detected using MASCaT of (C). *P*-values were
1022 calculated using chi-square test with Bonferroni's correction using mNeonGreen and
1023 Fas3G as controls, respectively. NS: $P > 0.05$, †: $P < 0.05$. Sample sizes are shown in the
1024 graph.
1025 **(E)** Western blot of adult male heads. Drice proximal proteins biotinylated by C-terminally
1026 knocked-in tagged V5::TurboID are purified using NeturAvidin.
1027 **(F)** A schematic model of subcellularly restricted non-lethal caspase activation at the plasma
1028 membrane (PM). Inactive Drice is in proximity to Fas3G in wildtype condition. *Fas3G*
1029 overexpression induces Dronc expression. Then, Dronc comes close to Fas3G and
1030 activates Drice. Activated Drice non-lethally cleaves substrate near PM including
1031 MASCaT probes.
1032

1033 **Figure 6**

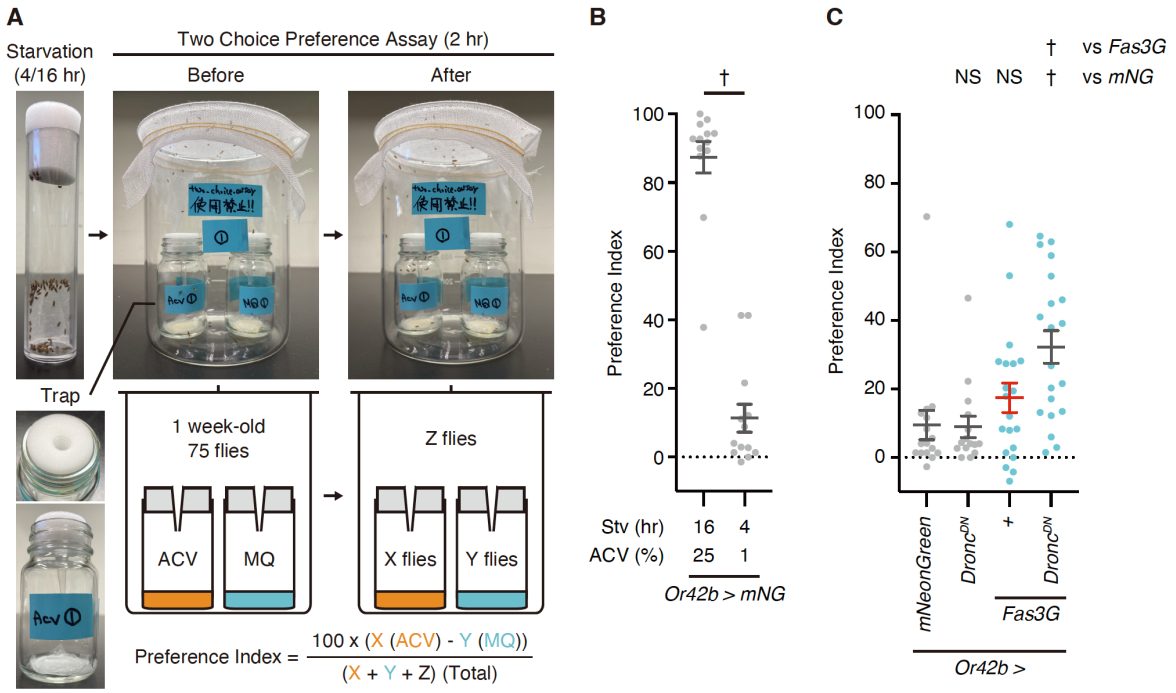

1034

1035 **Figure 6. *Fasciclin 3 isoform G* overexpression-facilitated caspase activation regulates**
1036 **attraction behavior.**

1037 **(A)** Images and schematic diagram of two choice preference assay. Flies are starved for 4 or 16
1038 hours before the assay. One week-old young flies are left for 2 hours in the bottle with 2
1039 traps. After the assay, preference index is calculated by counting the number of flies left in
1040 the trap with apple cider vinegar (ACV) as X, in the trap with MilliQ (MQ) water as Y, and
1041 other (field) compartments as Z.

1042 **(B)** Preference index of 1 week old male flies raised at 29°C. Flies are starved for 16 or 4 hours
1043 and are subsequently tested in response to 25% or 1% ACV in two choice preference assay.
1044 Data are presented as mean ± SEM. *P*-values were calculated using unpaired *t*-test. †: $P <$
1045 0.05. Sample sizes: 16 hr Stv/25% AC (N = 13 (915 flies)), 4 hr Stv/1% ACV (N = 13 (945
1046 flies)).

1047 **(C)** Preference index of 1 week old male flies raised at 29°C. Flies are starved for 4 hours and
1048 are subsequently tested in response to 1% ACV in two choice preference assay. Data are
1049 presented as mean ± SEM. Light blue dots represent *Fas3G* overexpression conditions
1050 while a red bar indicates caspase-activated condition. *P*-values were calculated using one-
1051 way ANOVA followed by Dunnets' multiple comparison test using mNeonGreen and
1052 Fas3G as controls. NS: $P > 0.05$, †: $P < 0.05$. Sample sizes: mNeonGreen (N = 16 (1159

1053 flies)), Dronc^{DN} (N = 15 (1099 flies)), Fas3G (N = 20 (1419 flies)), Fas3G + Dronc^{DN} (N =
1054 20 (1318 flies)).
1055

1056 **Legends for Table S1–7**

1057 **Table S1. Proximal protein list.** A list of the identified proximal proteins (Abundance ratio
1058 (Drice::V5::TurboID/Control) > 10). The UniProt Accessions, Gene Description, and
1059 Abundance Ratio (Drice::V5::TurboID/Control) are listed.

1060

1061 **Table S2. Gene Ontology analysis.** The result of Gene Ontology (GO) analysis of Cellular
1062 Compartment for Drice proximal proteins. GO term, P values, Fold Enrichment, Count and
1063 Genes are listed.

1064

1065 **Table S3. Fly stock list.** A list of the fly strains. Genotype, Map, Source or Reference and
1066 Stock# are listed.

1067

1068 **Table S4. Detailed genotypes.** Detailed genotypes and their related figure # are presented.

1069

1070 **Table S5. LC settings.** Gradient settings for LC analysis are presented.

1071

1072 **Table S6. MS/MS settings.** Settings used for the MS/MS analysis are presented.

1073

1074 **Table S7. Proteome Discoverer 2.2 settings.** Proteome Discoverer 2.2 settings for proteomics
1075 analysis are presented.

1076

1077